APPLICATION OF ELECTRICAL RESISTIVITY METHOD FOR GROUND WATER EXPLORATION IN SOUTH WESTERN BUTAJIRA AREA, GURAGHE ZONE

BY

BEREKET MEBRAHTU

MAY, 1997

APPLICATION OF ELECTRICAL RESISTIVITY METHOD FOR GROUND WATER EXPLORATION IN SOUTH WESTERN BUTAJIRA AREA, GURAGHE ZONE

A THESIS PRESENTED TO THE SCHOOL OF GRADUATE STUDIES OF ADDIS ABABA UNIVERSITY IN PARTIAL FULFILLMENT OF THE REQUIREMENT FOR THE MASTER OF SCIENCE DEGREE IN GEOPHYSICS

BY

BEREKET MEBRAHTU

MAY, 1997

ACKNOWLEDGMENT

I acknowledge the untiring efforts of my advisors Dr. Tigistu Hale, Ato Moges Tigabe and Ato Shimelis Fissiha, and all the members of Ethiopian Institute of Geological Survey specially those of Geophysics Department.

I am deeply grateful to Ato Sebsibe Alemneh and his Organization COWDO with its workers for supplying the technical support needed by partial sponsorship. I also thank very much W/t Genet Yifru COWDO's secretary, for typing the manuscript.

My thanks go to the department of Geology and Geophysics, AAU, for providing me all the necessary instruments for data collection.

I thank also the members of Geophysical observatory, AAU for their cooperation during my work.

Lastly but not the least, I thank very much my family and friends with out whose encouragement and support this project would have been impossible.

TABLE OF CONTENTS

ABSTRACT

The basic mathematical foundation for the vertical electrical sounding method has been presented by deriving the formula for the potential distribution at the surface of a horizontally stratified earth. The apparent resistivity and its relation with resistivity transform function has been shown particularly for Schlumberger Configuration. The theoretical background for resistivity inversion with the ridge regression technique has been explained following the method of Inman.

On the basis of the above theoretical consideration the electrical resistivity method has been applied for ground water exploration and possible site for borehole location in South Western Butajira Area, Southern Ethiopia. To do this survey along three profile lines were taken with a total of 20 VES points out of which 15 were analyzed in detail.

1. INTRODUCTION

There are several methods used in geophysical prospecting. Among these the **GEOELECRICITY,** deals with the electrical state of the earth including aspects related to the electrical properties of rocks and minerals under different geologic environments. It also discusses the influences of such electrical properties upon various geophysical phenomena.

Geoelectricty consists of various principles and techniques and makes use of stationary as well as alternating currents produced artificially or by natural ways. Among these diverse techniques, the one most commonly used for ground water exploration in an area with a layered ground surface of significant resistivity contrast among its layers is the **resistivity method.** The method has been widely applied for shallow and deep investigations. Several researchers (Long 1954; Van Nostrand and Cook 1966; Bhattacharia and Patra 1968; Apparoa and Roy 1971; Zohdy 1969; Zody, Anderson and Muffler 1973; Jain Kumar and Roy 1973; Kumar 1973a,b; Stanley, Jackson and Zohdy 1976; Patella 1977, 1978) have proved the suitability and effectiveness of this method by studying the response of diverse structures such as faults, dikes, vertical contacts, in the laboratory and in the field. It is a major tool used in surface ground water exploration efforts. Resistivity, the inverse of electrical conductivity is defined as the ratio of the voltage gradient to the current density over a small thin surface of a medium.

In a resistivity survey, a direct current (DC) or an AC of low frequency is sent through the ground between two metal electrodes. Because earth materials offer resistance to passage of current, some voltage loss will occur as the current flows from one electrode to another. The voltage loss (drop in potential) that occurs as the current moves through

the ground is measured at another pair of electrodes placed between the current electrodes.

The ability of a rock unit to conduct an electric current depends, primarily on three factors:

a) the amount of open spaces between particles (porosity),

b) the degree of interconnection between those open spaces which is described by the effective porosity, and

c) the volume and the conductivity of the water in the pores.

The presence of water and its chemical character are, therefore, the principal controls on the flow of the electric current since in nature most rock particles offer high resistance to electrical flow. It is found that , resistivity decreases with increase in porosity, hydraulic conductivity, water content and water salinity. Clay and shale have low resisitivities and dry sand and gravel have higher resistivities than saturated sand and gravel.. In general different rock types have different resistivities.

Resistivity values are obtained by two different surface exploration methods. The first of these, called the method of **electrical sounding,** involves vertical exploration. In this procedure a series of stations is established and careful depth soundings are taken. These soundings are later transferred to a vertical cross-section chart by evaluating the resistivity values from which understanding of the subsurface materials is obtained. This exploration method is especially useful for estimating the depth to sand, gravel, bedrock or water bearing strata, or for determining the thickness of selected formations. The electrical sounding method is, however, accurate only in the most simple geologic setting where the subsurface consists of horizontal layers parallel to the ground surface. The method was first applied by Conrads Schlumberger in 1912. An interesting description of the pioneer work of this investigator and his collaborators has been given by Kunetz (1966).

The second resistivity exploration technique is called **electrical profiling.** This method differs from that of the technique of electrical sounding in that only lateral variation in resistivity at a fixed depth is measured. As in the case of sounding, numerous stations ~~are~~ selected. Resistivity measurements are then made-this time for the same depth- at each station. These values, once plotted, produce a numerical picture of the subsurface materials at the chosen depth across a horizontal plane. Electrical profiling is most often used in searching for ore mineralized zones such as along dikes, faults or fault zones, for evaluating sand and gravel deposits, for delineating vertical boundaries of differing conductivity and for finding dipping contacts of different earth materials, for possible movement of water in hard rock terrain.

In addition, the electrical profiling methods have found wide applications in Engineering problems like location of weak zones in dam site investigations, etc.

In general, there are two most common electrode configurations to carry out the above survey procedures. These are:

1. The SCHLUMBERGER configuration, and
2. The WENNER configuration.

In the Schlumberger configuration, to change the depth range of measurements, the current electrodes are displaced outward while the potential electrodes, in general, are left at the same position. However, when the ratio of the distance between the current electrodes to that between the potential electrodes becomes too large, the potential electrodes must also be moved outward, otherwise, the potential difference becomes too small to be measured with sufficient accuracy. At the beginning of the series of measurements, the ratio of the potential electrodes spacing to the current electrode spacing may be taken as 1/3. Outward displacement of the potential electrodes is usually necessary

when the ratio has decreased to $1/_{20}$-$1/_{50}$. When the potential electrodes are displaced outward, it is necessary to carry out measurements at the two values of the potential electrode spacing, combined with the same value of the current electrode spacing. Preferably, these repeat measurements with a single value of the current electrode spacing and the two values of the potential electrode spacing should be carried out at two or three consecutive values of the current electrode spacing. This procedure will provide a reasonable amount of information on the effect of the displacement of the potential electrode upon the measurements.

One of the assumption on which the interpretation of resistivity sounding measurements is based on is that each of the subsurface layers is electrically homogeneous. One of the aspects which, in reality, differs from this simplified picture is that in many areas inhomogenities of small lateral extent occur close to the surface. These inhomogeneities distort the pattern of electrical current flow in their surroundings and consequently, if they are close to the potential electrodes, falsify the measured potential difference. This falsification occurs, of course, both in the Schlumberger and Wenner configurations. However, in the Wenner configuration the potential electrodes are displaced for each new measurement so that, the effect of near surface inhomogeneities is erratic or impossible to account for in the interpretation. In the Schlumberger configuration, on the other hand, the position of the potential electrodes is kept constant throughout a series of measurements so that similar errors occur in all the measurements. In this project, he main objectives of the survey are :

-to delineate subsurface layers of water saturation and their depths,

-to propose best sites for ground water bore hole locations,

-to study the general ground water potential of the survey area,

-to help in the geological study of the area by delineating the different geoelectrical formations from the geoelectric sections.

Since the general topographic features of the area and past geologic information suggest a flat lying sequence of alluvial deposits and weathered volcanic rocks, Schlumberger method of surveying was used to achieve the above objectives.

2. BASIC MATHEMATICAL FOUNDATIONS

2.1 The Potential Distribution at the Surface of a Horizontally Stratified Earth

To understand the relation between the quantities that are measured and the parameters that define the resistivity stratification in the subsurface and so to pave the way to a quantitative interpretation of the measurements, it is necessary to find the relation for the electrical potential at the surface of the earth. The derivation of this relation will be considerably simplified if one first considers the potential field at the surface setup by a single point source of current, because, in the derivation, the axial symmetry of the potential field can be utilized. Later, the potentials set up in the realistic case where two current electrodes are used can be found by algebraic addition of the potentials setup by a single electrode.

The case for which the potential will be derived below is defined by the following specification:

1. The subsurface consists of a finite number of layers separated from each other by horizontal boundary planes, the deepest layer extends to infinite depth, the other layers have finite thickness.

2. Each of the layers is electrically homogenous as well as electrically isotropic.

3. The field is generated by a point source of current that is located at the surface of the earth.

4. The current animated by the source is direct current (D.C.).

These specifications are also used as the basis for the interpretation of resistivity sounding data.

The derivation of the potential at the surface in the conditions specified above is due

to Stefaniscu et. al. (1930). Their derivation is presented below and in this derivation, the following should be noted:

a) The current density, denoted by J, is defined as the differential quotient of the current intensity passing through an area oriented at right angles to the direction of current flow with respect to that area.

b) The resistivity, denoted by (ρ), is defined as the resistance offered by an infinitesimal volume of cubic shape to a current flowing in a direction perpendicular to one pair of its faces, multiplied by the longitudinal dimension of that cube.

The current density J is related to the electrical field intensity E, by the relation

$$\bar{E}=\rho\bar{J} \tag{1}$$

which is Ohm's law for flow of electrical current in extended media.

The electrical potential, denoted by V, in D.C. conditions, satisfies the differential equation of Laplace which may be written in Cartesian coordinate as:

$$\frac{\partial^2 V}{\partial x^2}+\frac{\partial^2 V}{\partial y^2}+\frac{\partial^2 V}{\partial z^2}=0 \tag{2}$$

For the problem under the conditions specified above, the potential will have a cylindrical symmetry with respect to the vertical line through the current source and it would be appropriate to use the Laplace equation in cylindrical coordinates which is

$$\frac{\partial^2 V}{\partial r^2}+\frac{1}{r}\frac{\partial V}{\partial r}+\frac{\partial^2 V}{\partial z^2}+\frac{1}{r^2}\frac{\partial^2 V}{\partial \theta^2}=0 \tag{3}$$

If the potential is to be symmetrical with respect to the vertical coordinate axis (Z-axis), then equation (3) simplifies to

$$\frac{\partial^2 V}{\partial r^2}+\frac{1}{r}\frac{\partial V}{\partial r}+\frac{\partial^2 V}{\partial z^2}=0 \tag{4}$$

Particular solutions of equation (4) may be obtained by making the assumption that there exist solutions that have the form

$$V(r,z)=U(r)W(z) \tag{5}$$

If we substitute equation (5) into equation (4) and divide all terms over UW, then we obtain

$$\frac{1}{U}\frac{d^2U}{dr^2}+\frac{1}{Ur}\frac{dU}{dr}+\frac{1}{W}\frac{d^2W}{dz^2}=0 \tag{6}$$

This equation is satisfied if

$$\frac{1}{W}\frac{d^2W}{dz^2}=\lambda^2 \tag{7}$$

$$\frac{1}{U}\frac{d^2U}{dr^2}+\frac{1}{Ur}\frac{dU}{dr}=\lambda^2 \tag{8}$$

where λ is an arbitrary real constant.

The solutions of equation (8) are well known. They are

$$W=Ce^{-\lambda z} \wedge W=Ce^{+\lambda z} \tag{9}$$

The solution of equation (7) can be written as

$$U=CJ_0(\lambda r) \tag{10}$$

Combining equations (9) and (10), one obtains, as particular solutions of the differential equation (equation (4)),

$$V=Ce^{+z\lambda}J_0(\lambda r) \tag{11}$$

$$V=Ce^{-\lambda z}J_0(\lambda r) \tag{12}$$

In these equations, both C and λ are arbitrary constants.

Any linear combination of these particular solutions is also a solution of the deferential equation. Thus by making go through all possible values from zero to infinity and allowing the two constants to vary independent of λ , one obtains as the general solution of equation (4)

$$\int_0^{\infty}[\phi(\lambda)e^{-\lambda z}+\psi(\lambda)e^{+\lambda z}]J_0(\lambda r)d\lambda \tag{13}$$

where $\phi(\lambda)$ and $\Psi(\lambda)$ are arbitrary functions whose special forms are controlled by the

boundary conditions.

From elementary theory, the potential generated by a single point source of current of intensity I located at the surface of an electrically homogeneous earth is

$$V=\frac{\rho_1 I}{2\prod\sqrt{r^2+z^2}} \tag{14}$$

where ρ_1 is the resistivity of the homogenous earth and I is the current intensity.

Equation (14) can be written in a form similar to that of equation (13) using the well-known equation from the theory of Bessel functions, known as the Lipschitz integral. This equation is

$$\int_0^{\infty} J_0(\lambda r)d\lambda = 1/\sqrt{(r^2+z^2)} \tag{15}$$

Using this equation one may write equation (14) in the form

$$V=\rho_1 I/2\prod \int_0^{\infty}\exp(-\lambda z)J_0(\lambda r)d\lambda \tag{16}$$

The general solution of the differential equation (13) can now be written in the form

$$V=\rho_1 I/2\prod \int_0^{\infty}[\exp(-\lambda z)+\theta(\lambda)\exp(-\lambda z)+X(\lambda)\exp(+\lambda z)]J_0(\lambda r)d\lambda \tag{17}$$

where $\theta(\lambda)$ and X (λ) are arbitrary functions of .

Solutions of the form (17) are valid in all the layers in the subsurface, but the

functions of $\theta(\lambda)$ and $X(\lambda)$ are not necessary the same in the different layers of the subsurface. In the case of a point source of current at the surface of a horizontally layered earth we must thus write separate expressions for the solution in the different layers, i.e.

$$V_i=\rho_1 I/2\pi\int_0^{\infty}[\exp(-\lambda z)+\theta_i(\lambda)\exp(-\lambda z)+X_i(\lambda)\exp(+\lambda z)]J_0(\lambda r)d\lambda \tag{18}$$

where the subscript "i" refers to the several layers in the subsurface.

In this case, the following boundary condition must be satisfied:

1. At each of the following planes in the subsurface, the electrical potential must be continuous.

2. At each of the boundary planes in the subsurface the vertical component of the current density must be continuous.

3. At the surface plane, the vertical component of the current density and hence that of the electrical field intensity must be zero every where except in an infinitesimal neighborhood round the current source, and in view of condition (2) the vertical component of the current density must then also be zero in the ground at zero depth .

4. Near the current source, the potential must not approach infinite as $r \rightarrow 0$.

5. At infinite depth the potential must approximate to zero.

According to the condition mentioned under (1) at the depth h_i of the i^{th} boundary plane, the expressions for the potential (equation 18) in the i^{th} and $(i + 1)^{th}$ layer must be the same. This leads to the equation

$$\int_0^{\infty}[e^{-\lambda h_i}+\theta_i(\lambda)e^{-\lambda h_i}\chi_i(\lambda)e^{+\lambda h_i}] = \int_0^{\infty}[e^{-\lambda h_i}+\theta_i(\lambda)e^{-\lambda h_i}+\chi_i(\lambda)e^{\lambda h_i}]J_0(\lambda)d\lambda \tag{19}$$

This equation can only be satisfied for all values of r if the integrands on both sides of the equation are equal. One thus obtains the equation

Condition (2) leads to

$$\frac{1}{\rho_i}\frac{\partial v}{\partial z_i}\Big|_{h_i=0} = \frac{1}{\rho_{i+1}}\frac{\partial v}{\partial z}\Big|_{h_i=0}$$

Using equation (18) gives

$$=\frac{1}{\rho_{i+1}}\int_0^{\infty}[\{1+\theta_{i+1}(\lambda)\}e^{-\lambda h_i}-\chi_{i+1}(\lambda)e^{+\lambda h_i}]J_0(\lambda r)\lambda d\lambda$$

$$=\frac{1}{\rho_{i+1}}\int_0^{\infty}[\{1+\theta_{i+1}(\lambda)\}e^{-\lambda h_i}-\chi_{i+1}(\lambda)e^{+\lambda h_i}]J_0(\lambda r)\lambda d\lambda \tag{20}$$

Again, this equation can only be satisfied for all values of r if the integrands on both sides of the equation are equal and this leads to the equation

$$\frac{1}{\rho_i}[(1+\theta_i(\lambda)\}\exp(-\lambda h_i)-\chi_i(\lambda)\exp(+\lambda h_i]$$

$$=\frac{1}{\rho_{i+1}}[1+\theta_{i+1}(\lambda)e^{-\lambda h_i}-\chi_{i+1}(\lambda)e^{+\lambda h_i}] \qquad (21)$$

To satisfy the condition mentioned under (3), the expression for the potential in the first layer must be differentiated with respect to Z and then evaluated at Z=0 to get the equation

$$\int_0^{\infty}[-1-\theta_i(\lambda)+\chi_i(\lambda)]J_0(\lambda r)\lambda d\lambda=0 \qquad (22)$$

Here the first term is the **primary field** and it defines the field that would exist in a homogeneous earth and this field satisfies the boundary condition automatically. The last two terms together define the **perturbing field.** The vertical component of the field intensity of the perturbing field must be zero at the surface for all values of r, including that at the origin where the point source of current is located. This condition can only be satisfied if the last two terms of the integrand together are zero. This leads to the equation

$$\theta_i(\lambda)=\chi_i(\lambda)$$

The condition mentioned under (4) is automatically satisfied by the expression for

the primary potential. It is only necessary to make sure that the perturbing potential remains finite at the origin and thus does not influence the manner in which the total potential approaches infinity. The function $\theta(\lambda) = \chi(\lambda)$ remains finite throughout the range of integration and approaches to zero as $\lambda \rightarrow 0$. It then follows from equation (18) that indeed the perturbing potential can not become infinite at the origin. Hence, condition (4) is satisfied.

The condition mentioned under (5) requires that in the deepest layer, indicated by the subscript n, the function χ must be zero because, other wise, the factor e^{+z} would drive the potential to infinite value at infinite depth. This consideration yields the equation

$$\chi_n(\lambda) = 0 \tag{23}$$

The set of equations (20)-(23) provides a system of 2n equations in 2n unknown functions of $\theta(\lambda)$ and $\chi(\lambda)$. In principle, such a system of equations is capable of being solved. One is usually concerned, in particular, with the solution of the system for $\theta(\lambda) = \chi(\lambda)$ which, according to equation (18), defines the potential in the first layer, including the surface of the earth where the measurements are mode.

To obtain this solution, substitute equation (22) into the first of equations (20) and (21) and substitute equation (23) into the last of equations (20) and (21). For brevity, first introduce the following notations:

$$U_i = \exp(-\lambda h_i)$$

$$V_i = \frac{1}{U_i} = \exp(+\lambda h_i) \tag{24}$$

$$\rho_i = \frac{\rho_i}{\rho_{i+1}}$$

The system of equations then become

$$(U_1 + V_1)\Theta_1 - U_1\Theta_2 - V_1\chi_2$$
$$(V_1 - U_1)\theta_1 + \rho_1 U_1\Theta_2 - \rho_1 V_1\chi_2$$
$$U_1\Theta_2 + V_2\chi_2 - U_2\Theta_3 - V_2\chi_3 = 0$$
$$-U_2\Theta_2 + V_2\chi_2 + \rho_2 U_2\Theta_3 - \rho_2 V_2\chi_3 = (1-\rho_2)U_2$$
$$\cdots\cdots\cdots\cdots\cdots\cdots\cdots\cdots\cdots\cdots\cdots\cdots\cdots\cdots$$
$$U_{n-1}\Theta_{n-1} + V_{n-1}\chi_{n-1} - U_{n-1}\Theta_n = 0$$
$$-U_{n-1}\Theta_{n-1} + V_{n-1}\chi_{n-1} + \rho_{n-1}U_{n-1}\Theta_n = (1-\rho_{n-1})U_{n-1}$$

The solution of this system of equations for $\theta(\lambda)$ is obtained by the application of Cramer's rule. According to this rule, $\theta(\lambda)$ is obtained as the quotient of two determinants. The denominator of this quotient is

$$\tilde{D} = \begin{vmatrix} (U+V\cdot) & -U & -V & & \\ (U+V) & +\rho U & -\rho V & & \\ & +U & +V & -U & \\ & -U & +V & +\rho U & -\rho V \\ & \text{-------} & \text{----------} & \text{----------} & \text{---------} \\ & +U & +V & -U & \\ & -U & +V & +\rho U & \end{vmatrix} \qquad (26)$$

and the numerator is

$$\tilde{\rho} = -\begin{vmatrix} 0 & -U_1 & -V_1 & & \\ (1+\rho_1)U_1 & +\rho_1 U_1 & -\rho_1 V_1 & & \\ 0 & +U_2 & +V_2 & -U_2 & -V_2 \\ (1+\rho_2)U_2 & +U_2 & +V_2 & +\rho_2 U_2 & -\rho_2 V_2 \\ 0 & \cdots & +U_{n-1} & +V_{n-1} & -U_{n-1} \\ (1+\rho_{n-1})U_{n-1} & \cdots & U_{n-1} & +V_{n-1} & +\rho_{n-1}U_{n-1} \end{vmatrix} \qquad (27)$$

The determinant for **P** may be simplified by adding all the even columns to the first column, an operation which does not change the value of the determinant. This yields

$$\tilde{P} = \begin{vmatrix} -U_1 & -U_1 & -V_1 & & & \\ +U_1 & +\rho_1 U_1 & -\rho_1 V_1 & & & \\ 0 & +U_2 & +V_2 & -U_2 & -V_2 & \\ 0 & -U_2 & +V_2 & +\rho_2 U_2 & -\rho_2 V_2 & \\ 0 & - & - & +U_{N-1} & +V_{N-1} & -U_{N-1} \\ 0 & - & - & -U_{N-1} & +V_{N-1} & +\rho_{N-1} U_{N-1} \end{vmatrix}$$

For a two layer case, the matrices for **D** and **P** are restricted to the four elements in the top left hand corners of equation (27) and (28). Expanding the determinants, for this case, gives

$$\tilde{D} = (1+\rho_1) - (1-\rho_1)U_1^2$$

$$\tilde{P} = (1-\rho_1)U_1^2$$

Dividing numerator and denominator by $(1+\rho_1)$, and substituting for U_1 the expression according to equation (24) gives, for the two layer case,

$$\theta_1(\lambda) = \frac{\kappa_1 e}{1 - k_1 e^{-2\lambda h_1}} \qquad (29)$$

$(1-\rho_1)/(1+\rho_1)$. Similarly, for a three-layer case, the relevant matrices are the four by four matrices in the top left-hand corners of equations (26) and (28). Expanding the

determinants and dividing numerator and denominator over $(1 + \rho_1)(1 + \rho_2)$, results, for the three-layer case, the expression

$$\theta_1(\lambda)=\frac{K_1e^{-2\lambda h_1}+K_2e^{-2\lambda(h_2-h_1)}}{1+K_1K_2e^{-2\lambda(h_2-h_1)}-K_1e^{-2\lambda h_1}-K_2e^{-2\lambda h_2}} \qquad (30)$$

By equation (18) and (17) the potential at the surface of the earth, in conditions specified previously, is

$$V=\frac{\rho_1 I}{2\prod}\int_0^\infty[1+2\theta_1(\lambda)]J_0(\lambda r)d\lambda) \qquad (31)$$

This expression suggests that it may be desirable to consider a function K(λ)that is defined as

$$K(\lambda)=1+2\theta_1(\lambda) \qquad (32)$$

So that, the expression for the potential becomes

$$V=\frac{\rho_1 I}{2\prod}\int_0^\infty K(\lambda)J_0(\lambda r)d\lambda \qquad (33)$$

K (λ) is called **Slitcher's Kernel function** and $\theta_1(\lambda)$ is called the **Stefaniscu Kernel function** according to Koefoed.

2.2 The Apparent Resistivity Function

For an inhomogeneous medium, a quantity known as the apparent resistivity (ρ) is defined such that it is equal to the true resistivity of a fictitious homogeneous and isotropic medium which gives the same potential difference V as in the case of the inhomogeneous medium for the same current I and the same electrode arrangement.

In the ideal case of a homogeneous earth, the expression for the potential at a point on the surface of the earth that is caused by a point source of current located at the surface is

$$V_p = \frac{\rho I}{2\prod r} \tag{34}$$

where Vp is the potential caused by the point source, ρ is the resistivity of the homogeneous earth, I is the intensity of the current injected at the point source and r is the distance from the point source to the point where the potential is considered.

Consider a symmetrical linear electrode configuration with current electrodes on the outside, as illustrated in Fig 1. By equation (34), the potential difference between the measuring electrodes for a homogeneous earth is

$$\Delta V = 2\frac{\rho I}{2\prod}\left[\frac{1}{s-b} - \frac{1}{s+b}\right] \tag{35}$$

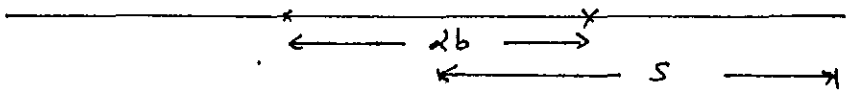

Fig 1. Illustration of rotation for symmetrical electrode configuration.

The expression for the apparent resistivity, ρ app, is then obtained by solving this equation for ρ. Thus

$$\rho_{app}=\frac{\Delta V}{I}\left[\frac{2\prod s(s^2-b^2)}{4bs}\right] \qquad (36)$$

The factor 2πs(s-b)/(4bs) here is termed as the **geometrical factor**, it depends on the type of electrode configuration used. To obtain the value of the apparent resistivity, the values obtained in the field measurement must be substituted in the right hand member of equation (36).

2.3 Apparent Resistivity For A Generalized Array

The potential at a distance r from a point source of current I on the surface horizontally stratified earth with homogeneous and isotropic layers is given by equation (33).

Equation (33) may be written as a convolution integral by making the following changes of variable

$$r=\exp(x)$$

$$\lambda=\exp(-y)$$

Then equation (33) becomes

$$V(r) = \frac{I\rho_1}{2\pi r}\int_0^\infty T(y)\exp(x-y)J_0[\exp(x-y)]\,dy$$

$$= \frac{I\rho_1}{2\pi r}\int_{-\infty}^{\infty} T(y)\,f(x-y)\,dy \qquad (38)$$

Thus, the potential is given by the convolution of the transform function with a so-called filter function which has the form

$$f(x-y) = \exp(x-y)\ J\ \exp(x-y) \qquad (38)$$

This convolution may be expressed in discrete form as (Rijo et al.1977)

$$V(r) = \frac{I\rho_1}{2\pi r}\sum_{j=-n_1}^{n_2} T(\ln r - \eta_j)\,C(\eta_j) \qquad (39)$$

where

η_j - are the filter coefficient abscissa,

$C(\eta_j)$ - are the digital filter coefficients,

n_1 - is the number of coefficients to the left of the filter origin,

n_2 - is the number of coefficients to the right of the filter origin.

Now consider the application of (39) to the generalized four-electrode array shown in Fig. 2, where P_1 and P_2 are potential electrodes, and C_1 and C_2 are current electrodes.

The potential difference between P_1 and P_2 is given by

$$V = V(r_{11}) - V(r_{12}) - V(r_{21}) + V(r_{22}).$$

Using (39) this becomes, for array configuration (or measuring point i,)

$$\Delta V^i = \frac{I\rho_1}{2\pi} \sum_{j=-n_1}^{n_2} T_{ij} C_j \qquad (40)$$

where

$$T_{ij} = \frac{\pi(\ln r_{11}^i - \eta_j)}{r_{11}^i} - \frac{\pi(\ln r_{12}^i - \eta_j)}{r_{12}^i} - \frac{\pi(\ln r_{21}^i - \eta_j)}{r_{21}^i} + \frac{\ln(r_{22}^i - \eta_j)}{r_{22}^i}$$

and

$C_j = C(\eta_j)$.

T_{ij} may be referred to as **the composite resistivity transform function**. It is a function of the earth model parameters and of the inter-electrode distances.

For the array shown in Fig 2, the apparent resistivity is given by

$$\rho_a = K\frac{\Delta V}{I} \qquad (41)$$

where

$$K = 2\prod \left[\frac{1}{r_{11}} - \frac{1}{r_{12}} - \frac{1}{r_{21}} + \frac{1}{r_{22}}\right]^{-1},$$

and is referred to as the geometric factor, whose value depends on the positions of the electrodes.

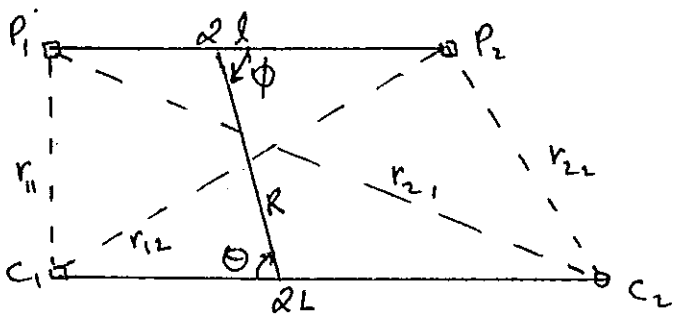

Fig 2. The generalized four-electrode array with potential electrodes P_1, P_2 and current electrodes C_1,C_2.(0<_,_<_)

Combining (40) and (41) one obtains an expression for the apparent resistivity measured by a generalized four-electrode array

$$\rho_a^i=[\frac{1}{r_{11}}-\frac{1}{r_{12}}-\frac{1}{r_{21}}+\frac{1}{r_{22}}]_i^{-1}\Sigma_{j=n_1}^{n_2}T_{ij}C_j \qquad (42)$$

Equation (42) shows that, for a given earth model, the apparent resistivity measured by a generalized array is given by the product of a geometric factor and a discrete convolution sum. The convolution serial products are formed from a set of composite resistivity transform values and an appropriate set of digital filter coefficients. The digital filter is seen to be independent of the electrode array.

2.4 The Digital Filter and Designing Techniques

Digital representations of the filter (38) have already been published. Koefoed et al. (1972) presented a 60-point filter for a sampling interval of (Ln 10)/10. Anderson (1979) published a computer programme to determine an appropriate filter length, he used a sampling interval of 0.2, i.e. (Ln 10)/11.513. Davis et al. (1980) presented a 34-point filter for a logarithmic sampling rate of six points per decade, i.e. (Ln 10)/6.

A sampling rate of six points per decade has become a widely accepted practice with resistivity surveying. The interpretation program used in this research uses a filter described by Davis et al. (1980). to calculate apparent resistivity curves for a variety of arrays and earth models

Although Davis's filter is not dependent on any array, his approach is array dependent in that a formula for apparent resistivity has to be derived for each array of interest. Apparent resistivity is expressed as linear combination of "monopole" resistivities which are obtained by convolving the filter with resistivity transforms. A "monopole" resistivity is essentially an electric potential multiplied by an inter electrode distance. This approach differs in that resistivity transforms are divided by the inter electrode distance prior to convolution with the filter to give an electric potential. The potentials for each electrode pair are summed to give a net potential difference, which is converted to an apparent resistivity by means of a geometric factor.

It has been shown that this filter performed very well under most conditions. Resistivity contrasts of around 500:1 were adequately handled for the Schlumberger array,

although significant errors were noted with the bipole-bipole arrays ($\theta = 30^0$), highlighting the array-dependent nature of the filter accuracy. This result is reported on a paper by D.J O'Neill and N.P. Merrick (1984). A further disadvantage of Davs's filter is its inapplicability to small machines.

With this problems in mind, O'Neill et al. decided there was a need for two additional filters: the first, for a logarithmic sampling rate of three points per decade, to overcome the problems of slow execution speeds (at the expense of accuracy) and the second for a rate of 12 points per decade, to provide sufficient accuracy in the case of models exhibiting large resistivity contrasts (with a corresponding decrease in execution speed).

Subsequent attention to the six-points-per-decade filter yielded a significant improvement over Davis's filter.

Several design techniques have been applied to the determination of filters for electrical and electromagnetic applications. For example, in the paper by Ghosh (1971 a), which gave rise to a subsequent proliferation of papers on digital linear filtering, a technique based on the Fourier transform was used. This scheme utilized the fact that the convolution in (37) can be represented by a multiplication of the Fourier spectra of input function and filter function to give an output function spectrum. Conversely, the filter function spectrum is obtained by dividing the output function spectrum by the input function spectrum. The filter function spectrum is then truncated at an appropriate Nyquist frequency (depending on the filter sampling rate), then transformed back to the space-time domain. Sampled values of the resulting (discrete) function constitute the required filter coefficients. As with other filter design techniques, the resistivity transform function is replaced by a known analytical input function associated with which is a known analytical

output function which satisfies (37).

The Fourier transform method has been criticized because it is relatively time consuming and requires a large amount of computer memory. Nevertheless, most of the published filters in this field have been derived by this method.

Johansen and Sorensen (1979) proposed a modification of the above technique, which claims to provide greater accuracy with reduced computational requirements, whereas Ghosh's use of a sinc interpolating function results in truncation of the filter spectrum at the Nyquist frequency with the resulting introduction of ripple into the filter, Johansen and Sorensen have proposed an alternative "sinsh" interpolating function which smoothly damps the high-frequency components of the filter, thereby reducing the unwanted ripple.

A technique based on a direct integration procedure has been published by Bichara and Lakshmanan(1976) and by Bernabini and Cardarelli (1978). Unlike the Fourier transform method, this technique can be applied only to certain types of filters. Its main advantage is that it requires minimal computer storage, although the rapid oscillations in the filter function make it difficult to obtain a sufficient degree of accuracy.

A generally applicable technique is the so-called Wiener-Hopf least-squares method, which is commonly used for the determination of shaping filters for the processing of reflection seismic data. Kefoed and Dirks (1979) were the first to point out the applicability of this technique to the determination of resistivity filters. The method involves adjustment of the filter coefficients so that the mean square of the differences between the actual filter output and exact filter output (as determined) by the output function being used) is minimized. A system of linear equations is obtained, with the filter coefficients as unknowns. A simple algorithm by Levinson (1949) allows efficient solution of the coefficients. The method used far less computer memory and time than the Fourier

transform method. It is explained clearly by Koefoed (1979).

Murakami and Uchida (1982) have proposed iteration on the least-squares method as a further improvement. The resulting filter is claimed to be shorter and more accurate than that provided by other design techniques, as a result of reduction of oscillation in the filter tails and minimization of round-off errors.

The derivation of the relation between the two based on equation (36). However, for the present purpose, the potential difference V is not obtained from the measurements but must be derived from the expression for the potential at the equation (33). Thus, V in equation (36) must be replaced by

$$V = 2 [V (s - b) - V (s + b)] \tag{43}$$

where the expression for V is taken from equation (33). This yields (using eqn.(36))

$$\rho \text{ app} = \frac{2\rho_1 s^2 - b^2}{4bs} \int_0^\infty K(\lambda)[J_0(\lambda s - \lambda b) - J_0(\lambda s + \lambda b)]\, d\lambda \tag{44}$$

or

$$\rho \text{ app} = 2\rho_1 \frac{s^2 - b^2}{4bs} \int_0^\infty T(\lambda)\,[J_0(\lambda s - \lambda b) - J_0(\lambda s + \lambda b)]\, d\lambda \tag{45}$$

Introducing the eccentricity C= b/s, this equation can be written as

$$\rho app = 2\rho_1 \frac{1 - c^2}{4c} \int_0^\infty T(\lambda)\{J_0[\lambda s(1 - c)] - J_0[\lambda s(1 + c)]\}\, d\lambda \tag{46}$$

2.5 Resistivity Inversion with Ridge Regression

The computer program used for interpretation of VES data in this research uses ridge regression inversion estimator to get a model that best fits the data in a least squares sense. This is explained below.

Marquardt (1970) and Hoerl and Kennard (1970a,1970b) propose a method called "ridge regression" that yields a better estimate of the unknown parameters than the method of least squares. Marquardt (1970) shows the similarities between the method of ridge regression and the method of the generalized inverse. He concludes that the method of ridge regression is preferable for problems with some very small eigenvalues, while the method of the generalized inverse is preferable for problems with some zero eigenvalues. Most resistivity problems involve small, but rarely zero, eigenvalues, hence Inman has abandoned the method of the generalized inverse for the more stable ridge regression method. However, the concepts of the information density matrix and the parameter resolution matrix as discussed by Inman et al (1973) and Glenn et al (1973) remain viable.

Apart from the problem of determining a model that fits the data, there exists the problem of estimating the accuracy of the parameters. In many soundings there is a range of parameters of a given n-layered model that fit the data accurately. While it is not always possible to predict exactly this range of the parameters, the method presented here which yields a good estimate of the range.

As was shown in the paper by Inman et al (1973), the problem of Schlumberger sounding over a plane-layered earth is nonlinear in the unknown parameters; Namely, the resistivity and thickness of each layer.

A Taylor's series expansion of first order in the unknown parameters is given as

$$\Delta P^* = (A^t A + kI)^{-1} A^t \Delta G, \qquad (49)$$

where I is the identity matrix and $k > 0$.

The eigenvalues of $(A^t A + kI)$ are $(\lambda_i^2 + k)$, where λ_2 are the eigenvalues of A'A. Any very small eigenvalues of the least-squares estimator will be increased in the ridge regression estimator by the factor k. Hence the inversion of the matrix $(A^tA + kI)$ will be more stable. Increasing the size of all the eigenvalues results in a significant decrease of (a) the mean of the squared length between ΔP and ΔP^* and (b) the variance of the estimated solution. So, in some cases, the solution ΔP^* is much closer to ΔP than the least squares solution ΔP. The residual sum of squares for the ridge regression solution is given by

$$\phi^* = (\Delta G^{**})^t \Delta G^* \qquad (50)$$

where ΔG^* is the measured resistivity minus the apparent resistivity theoretically predicted using the values $P^* = P^0 + \Delta P^*$. For a linear system, the residual sum of squares given by the ridge regression solution is greater than the residual sum of squares given by the least squares solution. Inman has found this not to the true for nonlinear systems. He has encountered many examples where the least-squares method diverges to give a very large residual sum, while the ridge regression method converges to an acceptable residual sum. Figure 3 illustrated some of there relationships for a general problem. The figure indicates the bias and the variance to the ridge regression estimator as functions of the parameter k. The point labeled "least squares" and the line labeled "ridge regression" are the squared

distances from ΔP to ΔP and to ΔP^*, respectively. The sum of the square of the bias plus the variance of the ridge regression estimator is equal to the squared distance from ΔP^* to ΔP. The figure shows that by allowing a small amount of bias in the solution we can realize a major reduction in the variance. For some values of k the ridge regression solution is much closer to P than the least-squares solution. This figure was drawn in reference to a linear problem, but the same behavior occurs for a nonlinear problem.

An important consideration is the choice of a value of k. In a linear problem the optimum value of k is that which gives the minimum mean-square error, namely, the value k* in Figure 3. However, this value cannot be determined unless the solution is known. Hoerl and Kennard (1970b) use a number of different values of k and then plot the solution versus k. They call this plot the "**ridge trace**"; the value of k for which it stabilizes being chosen as the optimum value. However, in the nonlinear problem several iterations may be necessary before a solution is obtained, and each iteration may require a different value of k. Marquardt's (1963) algorithm determines the smallest value of k for which the ridge regression estimator of equation (49) will yield a new model that better fits the field data. As the inversion process nears a solution or a minimum in the residual sum of squares [equation (50)], successively smaller values of k are used. It is worth noting that as k approaches infinity the ridge regression estimator in equation (49) approaches the gradient method. Convergence to a local minimum in the residual sum of squares is always possible with the gradient method (Ralston, 1965, pp.441- 442), but convergence is slow near the minimum. As k approaches zero, the ridge regression estimator becomes the least-squares estimator, equation (48), which is equivalent to the Newton-Raphson optimization technique. The Newton-Raphson technique converges very rapidly if it is near a minimum, but it may diverge if it is far from any minimum, one can see, therefore, that an optimum algorithm

would be one that resembles the gradient method when the estimator is far from the minimum and resembles the Newton-Raphson technique when the estimator is near the minimum. The ridge regression estimator has this property.

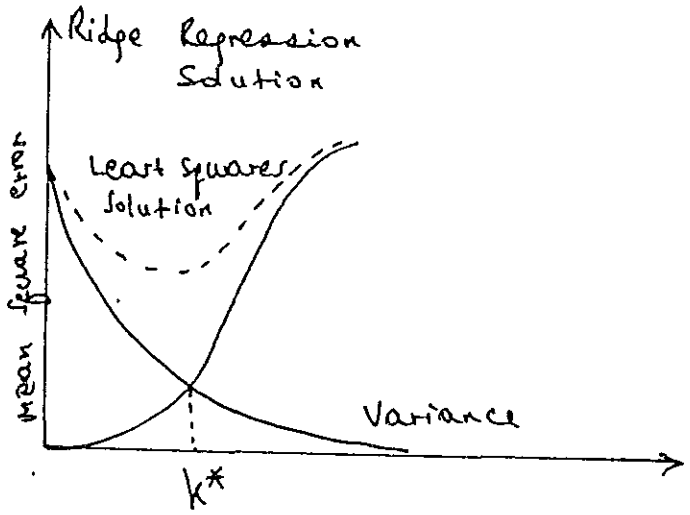

Fig. 3. Mean square error functions for the Ridge Regression estimator

(after Hoerl and Kennard; 1970 a)

The similarities between the ridge regression and the generalized inverse methods are given by Marqardt (1970). The generalized inverse method as applied to resistivity and electromagnetic sounding was described in the papers by Inman et al (1973) and Glenn et al (1973). The method begins by calculating the eigenvalues of the matrix ($\mathbf{A}^t\mathbf{A}$). Small eigen values indicate a near-singular system, which is unstable in the presence of noisy data. The reason is that when the inverse operation in equation (48) is performed, the eigenvalues are inverted, hence, the small eigenvalues have a large effect in the inverse solution. These small eigenvalues could result in a parameter change vector, Δ P in equation (48) that is so large that the linearization of apparent resistivity is no longer accurate. This usually results in an increase of the residual sum of squares. For this reason the generalized inverse

method works best when some of the very small eigenvalues are not included in the estimator. The addition of k to the diagonal elements of ($\mathbf{A}^t\mathbf{A}$), as is done in the ridge regression estimator, actually increase the value of each eigenvalue by the amount k, thereby increasing the size of very small eigenvalues. By increasing k, one has effectively reduced the number of eigenvalues included in the solution. As shown by Inman et al (1973), the data eigenvectors associated with the large eigenvalues tend to be smooth averages of all the data points, while the data eigenvectors associated with the small eigenvalues tend to represent averages of small groups of data points that correspond to detailed features in the sounding curve. If the small eigenvalues and their associated data eigenvectors are included in the estimator, the estimator will attempt to fit the more detailed features of the sounding curve as well as the broad features. However, if the residual sum of squares is far from a minimum and an attempt is made at the outset to fit the detailed features before obtaining a good fit of the broad features, the least-squares estimator will often diverge. Good results have been obtained using Marquardt's (1963) technique with a large value of k (on the order of 1.0) when the initial guess is far from the solution. A smaller value for k (on the order of .01 or less), which is equivalent to including the smaller eigenvalues in the estimator, is used near the solution.

Numerical Considerations

Evaluation of integrals

The system matrix A, equation (47) is comprised of derivatives of apparent resistivity with respect to the resistivity and thickness of each layer in the hypothesized model. A method similar to that of Mooney et al (1966) was used by Inman et al (1973) for evaluating both the forward problem and the derivatives. Although the method was

relatively fast for two-and three layer problems, it was too slow for four or more layers.

Several alternate methods are described by Cornille (1972) for evaluating Hankel transforms. The method used by Inman is to integrate numerically between zeros of the appropriate Bessel function and then sum the resulting terms which form an alternating series. If the resultant series is slow to converge, then Euler's transformation is performed. According to Inman in all problems encountered to date, it has never been found necessary to use more than thirty zeros of the Bessel function.

Weighting

When the data are weighted, a relative degree of importance is assigned to each value. Such weighting may be used to remove a bias inherent within the data or to bias the least squares fit so that it is more accurate in one area of the curve than another.

If there is a large numerical difference between the values of the data in different regions of the curve, an undesirable bias may be introduced into the final solution. The bias is such as to cause the ridge regression estimator to be biased toward the large values while for getting the smaller values, which may be as accurate and may contain some very important information.

For example, consider a simple two-layer model with a top layer of resistivity 10 ohm-m and a bottom half-space resistivity of 1000 ohm-m.The resistivity curve has two asymptotes with a large differences between the field curve and the curve generated from the estimated model. These differences would be greatest at the large array spacings merely be cause of the large numerical values of the curve in this region. The estimator would be more influenced by this portion of the curve than by the portion of the curve at the smaller array spacings. The estimator might then give a good estimate of the resistivity of the

lower half-space but a poor estimate of the resistivity of the first layer. In general, it is desirable to weight each data point according to the noise in that data point and, also, not give it a false degree of importance because of its large or small value in comparison with the other data points.

The weighting matrix **M** commonly used is

$$\mathbf{M} = \sigma^2 \mathbf{N} \tag{51}$$

$$= \sigma^2 \begin{vmatrix} \sigma_1^2 & \rho_{12}\sigma_1\sigma_2 & \rho_{1n}\sigma_1\sigma_n \\ \rho_{12}\sigma_1\sigma_2 & \sigma_2^2 & \rho_{2n}\sigma_2\sigma_n \\ \vdots & \vdots & \vdots \\ \rho_{1n}\sigma_1\sigma_n & \sigma_{2n}\sigma_2\sigma_n & \sigma_n^2 \end{vmatrix}$$

where

$$\sigma_i^2 = E(\epsilon_i^2), \text{ and}$$

$$\sigma_i \sigma_j \rho_{ij} = E(\epsilon_i \epsilon_j)$$

factor ρ is the correlation coefficient.

This matrix is the variance-covariance matrix of the data (Hamilton, 1964, p. 125). A first order approximation assumes that the error in the data at one array spacing is unrelated to the error in the data at another spacing, so that the variance-covariance matrix becomes a matrix with diagonal elements. To determine this matrix, it necessary to know the error in the data. In many nongeophysical problems the experiment is repeated several or many times in order to determine the error present. However, in most resistivity surveys the error must be estimated. Errors in the data come from several sources: limited precision

of instrumentation, effect of lateral inhomogeneities, telluric noise, and error in measuring spacing intervals. The term is called the **problem variance** and is commonly used when the relative variances are known or assumed within a scale factor, (Hamilton, 1964, p. 127). Inman's procedure assumes that each data point has the same percentage standard deviation unless it is known or suspected that certain points are significantly noisier. He further assumed, initially, that each point has a standard deviation equal to one percent of its measured value. The problem standard deviation is then adjusted to the estimated noise level of the survey. Most resistivity surveys yield data that is accurate within five percent or less.

To incorporate the weighting within the estimator, each side of equation (47) is multiplied by $\mathbf{N}^{-1/2}$. Neglecting the error vector ϵ one can write

$$\mathbf{N}^{-1/2}\Delta\mathbf{G} = \mathbf{N}^{-1/2}\,\mathbf{A}\,\Delta\mathbf{P}. \qquad (52)$$

The solution obtained using equation (52) is a weighted least-squares solution. The residual error is now defined as

$$\Phi = (\Delta\mathbf{G} - \mathbf{A}\,\Delta\,\mathbf{P})^{t}\,'\mathbf{N}^{-}\,(\,\Delta\mathbf{G} - \mathbf{A}\Delta\,\mathbf{P}) \qquad (53)$$

The weighted least-squares estimator is given by Jenkins & Watts (1968, p. 132) as

$$\Delta\mathbf{P} = (\,\mathbf{A}^{t}\mathbf{N}^{-1}\mathbf{A})^{-1}\mathbf{A}^{t}\mathbf{N}^{-1}\,\Delta\,\mathbf{G} \qquad (54)$$

and the regression estimator as

$$\Delta\rho^* = D(DA^tN^{-1}AD + kI)^{-1}DAN^{-1}\Delta G \qquad (57)$$

Equation (57) is the estimator that is used to provide a biased best fit to the Schlumberger sounding data.

It is interesting to note that the scaled matrix ($\mathbf{DA^tN^{-1}AD}$) is the matrix of correlation coefficients of the derivatives in the system matrix of equation (47) (Marquardt, 1963). Correlation coefficients that are nearly equal to unity indicate that the problem is highly non-orthogonal, or nearly singular. This will result in very small eigenvalues, a condition which renders the problem sensitive to errors in the data and to roundoff error in the computer, hence, it is necessary to add the factor k to the matrix ($\mathbf{DA^tN^{-1}AD}$) to stabilize the estimator.

Accuracy of Parameter Estimates

The emphasis in the previous sections was on the method for obtaining a solution by beginning at some initial guess significantly removed from the solution. In this section, methods for placing confidence intervals on parameter estimates and for assessing the final fit of the data will be described.

Residual variance

Prior to estimating the confidence intervals of the parameters, it is necessary to estimate the residual variance, or problem variance, in equation (51). An estimate of the

residual variance is given by Hamilton (1964, p.130) as

$$\sigma^2 = \frac{\Delta G^t N^{-1} \Delta G}{N-M} \qquad (58)$$

for weighted least squares. The only requirement to this point is that the values G(P, χ^i), the measured apparent resistivties, be unbiased finite variance estimates of the population means. If the measurement at a point were repeated an infinite number of times, the average value of all the measurements would be called the population mean. The fact that the number of points with a specified value increases as the value approaches the population mean indicates that the measured values have a finite variance. For purposes of simplicity it is assumed in this paper that each measurement is free of bias. This may not be strictly true in a Schlumberger array, where it may be common for the AB/2 spacing to be shorter than anticipated, but it is rarely longer. However, in many carefully conducted surveys this effect will probably be negligible.

The calculation of depends on the fit between the theoretical data, computed for the hypothesized model, and the field data. When is significantly greater than the data have not been fully explained by the hypothesized model. In many cases this means that more detail in the field curve may be fitted if a more complex model is used, such as one with more layers. However, a greater than may also mean that is underestimated. Although the value of varies between surveys, it is assumed that the error in any data point is five percent or less. If is found to be greater than either the estimated variances of the observations have been overestimated (Wiggins, 1972 p.258-259) or the curve calculated

from the hypothesized model is fitting the noise in the data.

Thus, one sees that the residual variance can be used as an indication of the goodness of fit given by the hypothesized model (Glenn et al, 1973). The residual variance is independent of the linearity or non-linearity of the problem with respect to the model parameters.

Covariance of Parameters

It is important to be able to judge the accuracies with which the parameters of the estimated model are known. It was noted earlier that it is very difficult to determine accurate estimated for the parameter standard deviations if there is a high degree of correlation between the parameters or if the problem is nonlinear in the estimated parameters. Also, there is the problem of calculating the variance of a biased estimator [equation (57)] and interpreting the variance in terms of the earth model. While it would be nice to be able to give a firm, quantitative answer to the question of parameter standard deviation, it is impossible to do so. Hence, in the following paragraphs the philosophy Inman used to make a conservative estimate of the parameter standard deviation will be presented.

One of the first problems encountered results from the fact that the variance of the ridge regression estimator decreases with increasing k (Figure 3). Increasing the value of k is similar to disregarding the small eigenvalues and their associated eigenvectors of the system matrix **A** of equation (52). Each eigenvector is a linear combination of the original parameters of the model (resistivity and thickness), and those parameters associated with the largest eigenvalues are the best determined linear combinations. This means that if one calculates the variance of equation (57), the biased estimator, the standard deviations for the original parameters will be unusually small because the linear combinations of the

parameters with large variance have been neglected. In effect, the variance of the biased estimator is a poor estimate of the true variance of the original parameters.

For example, suppose a field curve is measured over a layered earth that has a thin conductive layer. Among the eigenvectors associated with the largest eigenvalues there will be one eigenvector which represents the resistivity-thickness product of the thin conductive layer because this product is well defined by the Schlumberger sounding curve. Among the eigenvectors associated with the smallest eigenvalues there will be one eigenvector which represents the ratio of thickness to resistivity of the thin conductive layer because this ratio is poorly defined by the Schlumberger sounding curve. Thus, while the product is well determined because it is associated with a large eigenvalue, the ratio is poorly determined because it is associated with a small eigenvalue. If a biased estimator, which eliminates the small eigenvalues and the associated eigenvectors, is used, then the variance estimate would be quite small because of the well-determined resistivity-thickness product. Although a solution is obtained using a biased estimator, the variance of the parameters is computed with the least-squares estimator, which is not biased.

The least-squares estimator, equation (56) includes all the eigenvalues, and, therefore, the parameter variance should be calculated from this expression. The variance-covariance matrix, cov (ΔP), is

$$\text{cov}(P) = D(DA^tN^{-1}AD)^{-1}DA^tN^{-1}.\text{cov}(G)N^{-1}A^tD(DA^tN^{-1}AD)^{-1}D \qquad (59)$$

The covariance matrix of G is given in equation (48) as σ N. The covariance of P now becomes

$$cov(\Delta P)=\sigma^2(A^tN^{-1}A)^{-1} \qquad (60)$$

The value of is estimated by equation (56). Equation (60) is a matrix whose diagonal elements are the variance terms of each element of the vector ΔP and whose off-diagonal elements are the covariance terms between the elements of ΔP.

The next question is one of relating the covariance of ΔP to the covariance of the model parameters P. Note in equation (54) that the vector contains the predicted parameters ΔP and the estimated parametersΔP^0. SinceΔP^0 is known, any large variance in ΔP corresponds to a large variance inΔP (Glenn et al, 1973). Thus, the covariance of P may be written as

$$cov(P)=\sigma^2(A^tN^{-1}A)^{-1} \qquad (61)$$

The correlation matrix is an indication of the linear dependence between the parameters. The elements of the correlation matrix are given as (Jenkins and Watts, 1968, p.74)

$$[cor(P)]_{ij}=\frac{[cov(P)]_{ij}}{[cov(P)_{ij}]^{1/2}[cov(p)]^{1/2}_{jj}} \qquad (62)$$

If the value of [cor(P)] is near unity, then the parameters r_i and t_i correlated and linearly dependent.

Solution Space

The diagonal elements of the covariance matrix are the variance tern parameter. If the correlations are small then the standard deviation is a good the uncertainty of each parameter. If two parameters are strongly correlated standard deviations given by the square roots of the diagonal terms of (61) will than the actual uncertainties. This fact is illustrated in Figure 4 which is a ge section in solution space. The two coordinate axes correspond to two paramete estimated earth model. The ellipse indicates a confidence region within which the sum of squares may be expected to lie for a certain percent of the repeated expe This region also defines the values of the parameters p_2 and t_2 which will give a within the contour. The origin of the axes is defined by the parameter values dete from the final solution. The tilt of the axes of the ellipse is a measure of the de correlation between the two parameters.

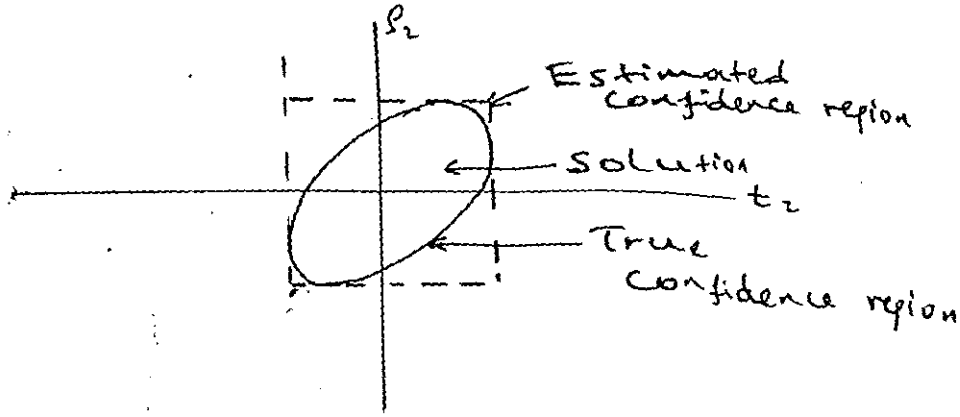

Fig.4 Hypothetical solution space for a thin conductive layer.
The contour defines a confidence region.

If the standard deviations of the diagonal terms of equation (61) are taken to be the true deviation estimates, then the ellipse of Figure 2 is enclosed by a box whose sides are defined by the standard deviations. It is easy to see that the box, which does not allow for the correlation between the parameter, represents a much larger confidence region than the ellipse, use of the box limits leads to a conservative estimate of the parameter confidence intervals. A useful practice is to present both the covariance matrix and the correlation along with a "slice" of solution space. We normally take a slice defined by the parameters with large correlations, these parameters are usually the resistivity and thickness of a thin layer. Each point in the slice represents the parameters of a particular model, and at each point the least squares error between the sounding curve defined by the model and the field curve is calculated. The values can then be contoured into confidence regions defined by (Jenkins and Watts, 1968, p.138)

Where $\Phi(P)$ is the least-squares error that defines a particular confidence interval and (P) is the least-squares error at the minimum (or solution) in solution space. The quantity $F_{M,N-M}(1-\alpha)$ is the value of the F-distribution for M and N-M degrees of freedom at the 1 - confidence level. The value (P) defines a region in solution space in which there is a $100(1-\alpha)$ percent chance of a repeated experiment yielding a value for (P) within this region. Shuey (1973) and Schellinger (1972) discuss the use of these contours in reference to interpretation of gravity and magnetic anomalies, respectively. The solution space enables the investigator to determine the range of models that fits the data.

3. APPLICATION OF THE ELECTRICAL RESISTIVITY METHOD FOR GROUND WATER EXPLORATION IN SOUTH WESTERN BUTAJIRA

As can be understood from the title of this thesis research, the second part consists of collection, analysis and interpretation of data from the specified site.

The procedures of investigation, i.e. data collection, methods of analysis and results are reported in this section.

Collection of data was carried out first by preparing a work plan. In the plan three profile lines and an average of six VES points were selected on each profile .

It is known that the depth of current penetration varies with the current electrode separation, so the procedure in the field is to use a fixed center with an expanding spread. This technique is particularly suited to detect the presence of horizontal or gently sloping beds of different resistvities, and in this respect it is often used to determine:

i) the depth of over burden,

ii) the depth to the water table,

iii) the depth, structure, and resistivity of different underlying beds,

The main equipment in carrying out the resistivity measurements include a power source (generator), a current transmitter, a receiver for measurement of potential difference, electrodes, cables and reels. The power supply can either be DC or a low frequency (less than 60 HZ) AC. In cases where portability is given precedence, a set of batteries as required by the particular equipment in use and may be connected in series to give the necessary supply. Otherwise, a motor generator having a capacity of several hundred watts

is preferable for large scale work. It is customary to periodically reverse the polarity of the D.C. in order to avoid effects of electrolytic polarization caused by the flow of current in only one direction.

In addition to the use of low frequency AC or rapidly interrupted DC to eliminate the spontaneous potential effect, narrow band amplifiers tuned to the source frequency are employed to increase the signal-to-noise ratio; however, this will give a resistivity lower than the true resistivity value.

Other serious problems that may be encountered are inductive coupling between current and potential cables, current leakage especially on the ground, and these effects increase with frequency.

3.1 The Survey Area

3.1.1 Location and Accessibility

The survey area is located in central southern part of Ethiopia, currently in Southern Ethiopia regional administration, in Guraghe zone, in Meskanena Mareko and Silte Wereda which is in close proximity to South-South-West, 12kms from Butajira town. It is composed of nine peasant associations (Gideyna Aborat, Wouribe, Mikaelo, Yeteker, Mirab Embore, Misrak Meskan, Misrak Embore, Merab Meskan and Agode Lobrera), lies between $8^0$01' and $8^0$07'30" latitudes North and $38^0$15'30" and $38^0$23' longitude and is the target area for RURAL COMMUNITY WATER DEVELOPEMENT ORGANIZATION(COWDO)which has been doing ground water developments in the area.

The survey area is accessible via 145 km all weather gravel road through Alemgena or Via 160 km asphalted road upto Zway and 50 km all weather gravel road to the town of Butajira. There are dry weather roads from the main road to all peasant associations.

Fig. 5. LOCATION

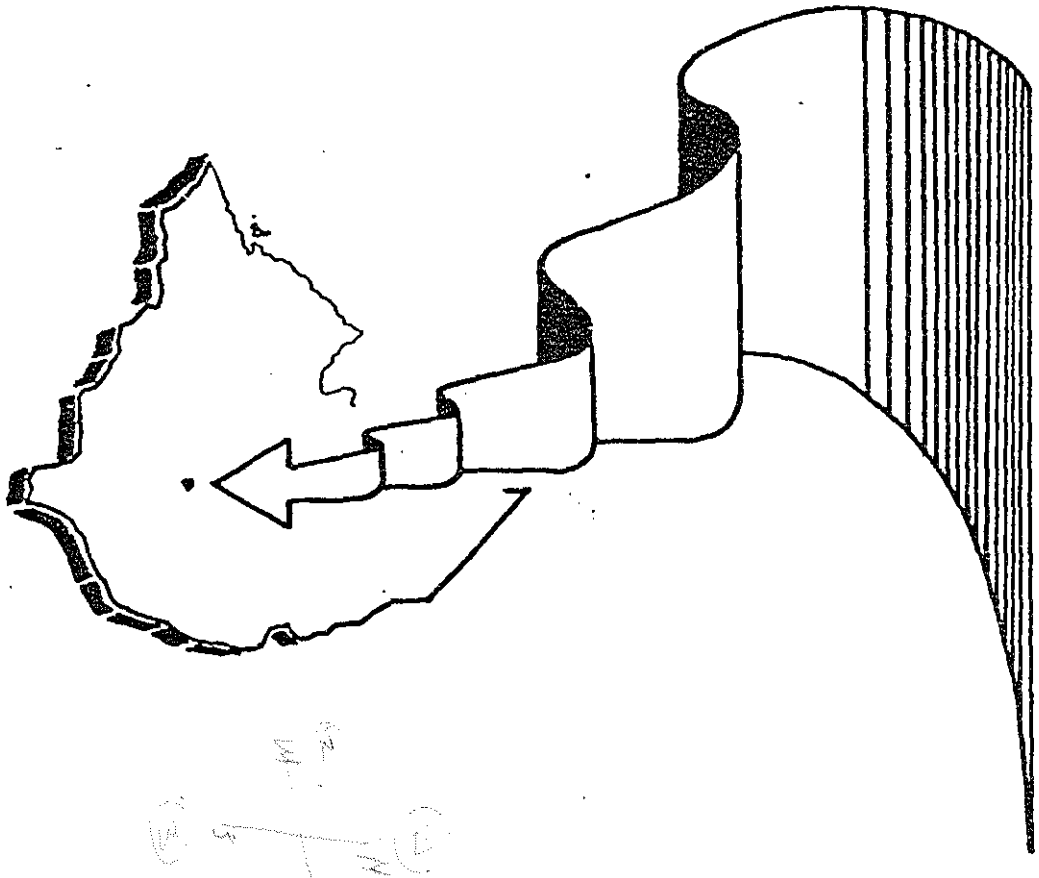

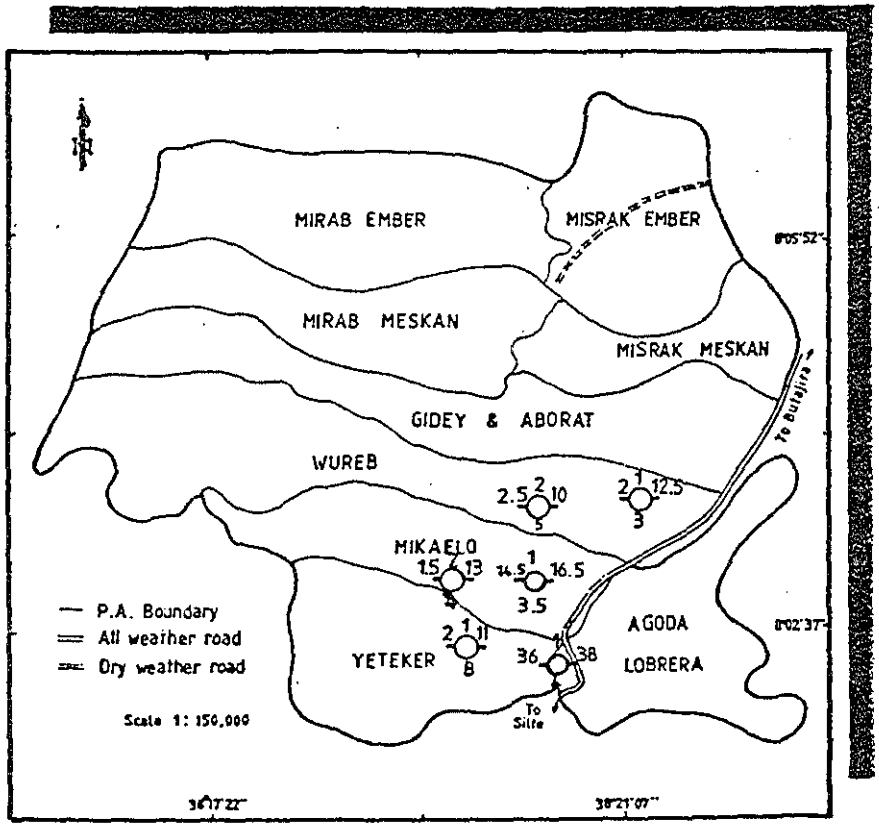

KEY

HAND DUG WELL D A B C

A Reference number

B Total depth

C Estimated yield in m^3/day

D Static water level

3.1.2 Natural Condition of the Survey Area

Climate and Vegetation

According to Makin, M.J. et al (1975) the southern rift valley in Ethiopia may-be classified into three eco-climatic zones: humid to dry sub-humid lands dry sub-humid or semi-arid lands and semi-arid and arid lands. The survey area and its vicinity can be classified as humid to dry sub-humid lands. The mean annual rainfall ranges from 1000-1100 mm and the mean seasonal temperature ranges from 15 to 20^0c.

The main vegetation type covering the target area is tropical wood land and thornbush, scattered small shrubs and low acacia (grar, lafto) trees in a ground cover of grasses. These are mainly available in the vicinity of the escarpment which is the western boundary of the main Ethiopian rift.

The Western highlands of the escarpment have relatively denser vegetation cover than the low land since the high population density has resulted in great deforestation. Normally the steeper the slopes and cliffs, the greater is the density of the forest.

Geomorphology

The Western part of the survey area is bounded by the western rift escarpment of high land volcanic landforms associated with major faults trending NN-E and having elevation ranging from 2200-3100 m.a.s.l. The Eastern part is bounded by volcanic remnants trending NN-E and having elevation ranging from 2200-2500 m.a.s.l. The major part, which is the central part of the survey area, is a residual volcanic land form, undulating and rolling low land topography and having an average elevation of 2140 m.a.s.l and it is the down thrown part of the major fault system.

Soil

Clay soil, which is derived from Ignimbrite in-situ and/or transported from the high land, generally cover the survey area. The thickness of the soil is variable, it is mostly less than 2 meters. Deep cuttings in soils have been developed due to degredational action and which can be classified as a region of high soil erosion.

Drainage

The survey area lies in the lake basin.. The western escarpment of the high land which is trending NN-E is its major surface water divide. The drainage patterns are generally parallel to sub-parallel and angular to sub-angular and which are flowing to east-west direction having III order and controlled by fracture and/or fault systems.

3.1.3 Geology of The Survey Area

Ethiopia, as a whole, can be divided into four physio graphic regions widely known as the North Western plateau, South Eastern Plateau, the Main Ethiopian Rift and the Afar depression.

The target area is part of the Main Ethiopia Rift particularly its the southern part. Its geology consists of two main volcanic formations.

1.The Magdala Group (upper miocene, pleistocene)

This volcanic rock of the Magdala group covers a very wide area in the central part of Ethiopia, especially in the Rift and sometimes outside of the Rift. This group of volcanic rocks consists of rhyolites, trachytes rhyolitic and trachitic tuffs, ignimbrites, agglomerates, and basalts. The thickness of this volcanic sequence is more than 1km.

2.The Alkaline, Olivine Basalts (Q6)

This group of volcanic rocks overlies the Magdala group as sills and flows. The area they cover ranges from few km^2 upto some hundreds km^2. According to V.V. Pilat, the thickness of this basalt is not very big, and is not more than a hundred meter.

The target area has quaternary sediments also and these sediments (Q, Qp, Qh) are of different genetic types (flivial, lacustrine, eolian, eluvial, marine). They are widely spread all over Ethiopia. In the Ethiopian Rift System, the Quaternary sediments are mostly of lacustrine origin. Lacustrine beds are interbedded with Plio-Pleistocene ignimbrites in the lakes region and on the rift shoulder (Mohr, 1966, Lioyd, 1980). The lacustrine beds are mostly re-deposited volcanic sands, tuff with calcarious material and diatomite. According to Mohr (1966), at the beginning of the Quaternary, an ancestral lake which was almost certainly continuous from the Abaya and Chamo lakes to the South to the Awash basin to the North existed until it was separated by late Pleistocene tectonic movements.

3.1.4 Hydrogeology of The Survey Area

The rock type (formation) of the Butajira region is lacustrines and swamp deposits, volcano lacustrine deposits of the rift floor.

Water in the zone of saturation is the only part of all subsurface water which is probably referred to as ground water. The saturation zone may be viewed as a huge natural reservoir or system of reservoirs, whose capacity is the total volume of pores or opening in the rocks that are filled with water.

Ground water may be found in one continuous aquifer system or in several separate (discontinuous) aquifer systems in the survey area.

The hydrogeology of the study area has been classified into three aquifer systems with their relative productivity (Sebsibe Alemneh, 1994).

1. High productive, intergranual aquifer from weathered ignimbrite and/or tuff.-
2. Medium productive, fissured aquifer from ignimbrite

1. High land areas with no essentially water resource.

1.High productive, intergranular aquifer from ignimbrite and/or tuff

This aquifer system is situated along all the high land rift escarpment in western part of the target area. The high fracturing and faulting density which are the result of tectonic activities, of this aquifer system have made to have locally high permeability and productivity. This is evidenced by several springs emerging locally along the major fault line at the foot of the rift escarpment. These springs are yielding in the range of 0.5-3 lit/sec. Shallow ground water at the foot of the escarpment and its vicinity could be locally developed by hand dug well from the same aquifer system.

2.Medium productive, fissure aquifer from ignimbrite

This aquifer system is the most extensive portion of the survey area which is the central and topographically the lowest part. It has an extensive and continuous ground water flow system within a porosity between the individual grains. Shallow ground water in the area ranges between water table and semi-confined conditions, but it mostly under water table aquifer conditions and depth to ground water ranges from 6-30 meters depending on the local topography.

3. High land area with essentially no water potential

This system comprises relatively less or no permeability of the western high land rift escarpment and the recent basalt and/or scoria domes. Particularly the scoria and scoraceous basalt (s) show no drainage on their slopes as they have high permeability, however, their topographic nature do not favor for groundwater development.

Aquifer characteristics of different rock units of the Butajira area especially that of the lacustrine deposits (Q_1) as explained by Tesfaye Chernet (1993) is given below.

1. Cenozoic Sediments

1.1 Lacustrine deposits (Q1) are lacustrine and swamp deposits and volcano lacustrine deposits of the rift floor. Most of the lacustrine sediments are located around existing lakes because they were deposited when these lakes were much larger in size during the pluvial times. The most extensive lacustrine sediment are known in the Lakes Region of the Rift Valley south of Addis Ababa. This includes the area between lake Koka, and Lake Shala to the South, around Lake Awassa, around Lake Abaya, and the area around Lake Turkana and Lake Chew Bahir . In the highlands, extensive outrcrops of lacustrine sediments occur only around Tana.

The lacustrine sediments show a lot of differences in their permeability, those showing the high permeability are the ones consisting of volcanic sands, water lain volcanic sands (such as those around Debrezeit and Metahara). Some of them are known to provide more than 10lit/sec for no draw down. On the other hand, fine grained sediments with interbedding of massive tuffs and fine ash are also known to exist. As a whole, the lacustrine sediments may be taken to have a moderate or high permeability & productivity and the permeability is of intergranular type. The main problem of developing ground water in lacustrine sediments is that of encountering waters with high salinity and for the

high fluoride content especially in the rift valley. The lacustrine sediments are situated in low lying areas and they store large quantities of both fresh and saline ground waters.

From general experience found in the survey area, it is known that hand dug wells or boreholes in the lacustrine sediments strike ground water in less than 50m depth and in general give yields between 1 and 5 liters/sec (even much more in some cases).

Surface Water

Several springs start specifically from the western high land rift escarpment and jointly flow as two major perennial streams to the east and join to River Meki and enter to Lake Ziway. Along their course they partly recharge the shallow ground water regime depending on topography. Their discharge range from 0.5 to 3 lit/sec (Sebsibe Alemneh (1994)).

3.1..5. Recharge, Discharge & Ground Water

Movement Conditions

The high land escarpment zone and zones along fractures and faults are the main recharge area. At the foot of the escarpment and the central low land area are the ground water discharge area. The recharge systems mainly in the central low land area is accomplished by base flow from streams, along the fracture and faulted zone of the high land escarpment and from direct precipitation.

Ground water movement of the target area is, generally, supposed to be towards the east. Between the months of June and August unlike of the Springs, ground water table at the lowlying central part of the target area rises to the depth of few centimeters to one meter.

3.1.6 Hydrochemistry of The Survey Area

Representative ground water sample were collected both from the high land rift escarpment zone and low-lying central part of the target area and chemically analyzed by Sebsibe Alemneh (1994). According to the results of his research, Total Dissolved Solid (TDS), pH and fluoride values of the ground water range from 350-550 ppm, 7-7.5 and 0.1-0.3mg/lit respectively, which are within the recommended limits of drinking water standards by World Health Organization (WHO).

4. DATA COLLECTION, INSTRUMENTS USED, ANALYSIS AND INTERPRETATION TECHNIQUES

4.1. Data Collection and Instruments Used

Data was collected between January 26 and February 6, 1997 for twelve days. Three profile lines running from East to West were selected. The distance between any two of these profiles was three kilometers. On each profile, an average of 7 VES points were selected so that there would be a total of 20 VES measurements. But due to different reasons, only 15 VES measurements were considered for analysis. These points are located in figure 4 . They have approximately the same azimuth (i.e. N-S). The maximum current electrodes separation (AB) attained varied from 300m to 1km with an average value of about 600m. The corresponding depths of investigation are estimated to be between 100m and 200m. Three potential electrode distance (MN) were used for each VES. These were one meter, twelve metro, and ninety metro.

Field data is composed of instrument readings voltage (V_p) from the receiver and current (I) from the transmitter. These readings were used to calculate apparent resistivity values (ρ_a) using the relationship $\rho = KV_p/I$. where K is a geometric factor.

The instruments used were TSQ-3 square valve transmitter. IPR-8 potential receiver, 8HP Brigg and Strattonmotor generator, six stainless steel and iron electrodes, two reels each with half a kilometer length insulated wire for current and potential line, hammers, plastic tapes, and other accessories.

4.2. Data Analysis

The complete interpretation procedure for sounding data is first to use the two-layer plus auxiliary curve matching method to get a semiquantitative estimate of the vertical electrical variation and then input that resistivity section and compute its theoretical sounding curve. This procedure is repeated until an acceptable fit between the field curve and the theoretical one is obtained. At this stage of the interpretation it is necessary to incorporate into the resistivity section an information obtained from seismic, geological, hydrogeological and bore-hole(well-log) investigation or others available.

Interpretation by the curve matching technique is practicable only when the number of layers is small, say upto 4. Even for four layers the number of reasonable parameter combination is 50 large and the collection of curves bulky that interpretation by matching becomes generally impracticable and for a large number of layers, it is virtually impossible. In addition to this technique is time consuming and not reliable. Fortunately, modern developments in geophysical theory ,instrumentation and electronic theory have rendered the curve matching technique largely obsolete.

The interpretation process is highly facilitated by using a computer. Since 1973 various authors have published methods of automatic interpretation in which the computation of the layer parameters are made by the computer. At present the interactive and automatic methods are the most widely applied tools in the interpretation of resistivity

soundingmeasurements.

The programwhich is usedfor datainterpretationin this researchis calledRESIX plus prepared by Interpex Limited Golden, Co. and supplied by COWDO. It is an interactive, graphically oriented, forward and inverse modeling program for interpreting resistivity sounding data interms of a layered earth (1-D) model. In the interpretation program, data is entered as apparent resistivity versus spacing. Forward modeling allows the user to calculate a synthetic resistivity sounding curve for a model with up to six plane layers. Resistivity sounding curves are calculated using linear filters in the manner described by Davis, et al (1980).

In this work, shifting of data with overlapping segments was handed manually by making the data curve to meet either the longest or shortest spacing segment while direct inversion allowed the researcher to estimate the layered model directly from the data curve, without having to manually construct the number of layers and layer resistivity and thickness. This is done using a method similar to that of Koefoed (1976). Ridge regression inversion of the data using the direct inverse results (estimated model) was done, as the estimated model doesn't fit the data as well as it could.

Inverse modeling allowed the researcher to obtain a model that best fits the data in a least squares sense and this was done using the ridge regression technique (Inman,1975). The starting models for the inversion were produced automatically using the estimate command. These models had upto six layers. Forward models had up to five layers.

Equivalence analysis allowed the researcher to generate a set of equivalence models, that is, alternative models that fit the data nearly as well as the best fit model, but differ from this model. Equivalence analysis also indicated the allowable range of each of the model parameters. It was done for some of the VES data.

Results from forward or inverse modeling were directed to a Laser Jet printer for report ready. The results are also saved in a binary random access disk file for later retrieval. These results were also used to construct geo-electric sections and pseudosections for the three profiles using soft wares.

5. RESULTS, DISCUSSIONS AND CONCLUSIONS

5.1. Results and Discussions

In all of the geo-electric section for the three profile, it can be seen that there is a thin geo-electric layer of low resistivity whose thickness varies from few centimeter upto about one meter next to this, there is a relatively thicker electrical layer of higher resistivity than the first layer. Then a very thick geo-electrical layer whose resistivity is between 10-80Ω-m covers most of the area. Its lateral extent is also very large. The thickness of this layer can not be exactly known. But gradually decrease towards the east. Next to this later, at the eastern bottom of the geo-electrical sections, a layer of the highest resistivity whose thickness increases towards the east can be seen. As we go Northward starting from profile 1 towards profile 3, we can observe that the bottom layer shows gradual decrease in thickness and ultimately thins out at profile 3.

Profile 1

For this profile, there is a first geo-electric layer whose resistivity varies from 10-20 Ω-m and low and have an average thickness of about 50m. This layer thins out as we go toward cost. it may be a recently deposited alluvial deposit. It may be composed of sand clay and gravel sediments underlying this, there is a second geo-electric layer of larger thickness. Its resistivity varies from 20-30 Ω-m. It has a maximum thickness of about 200 m on the Western part of the geo-electric section. The minimum thickness is about 50m on the eastern part of the electric section. This layer is exposed at the surface on the eastern part. This layer is the most probable aquifer as there lies a less compact permeable geo-electric layer above it and on impermeable layer of higher resistivity beneath. Hence this bed may offer an ideal situation for accumulation of ground water. On this profile, there is a third geo-electric layer of relatively higher resistivity (which is greater than 80 Ω-m).

Thickness of this layer varies from about 30, on the Western side to above 250m on the Eastern side of the geo-electric section. This layer may be composed of weathered alkaline and olivine basalt. Its higher resistivity shows that it is an impermeable layer.

Profile 2

This profile consists of the total number of layer present. The first geo-electric layer is not composed of more than one material. It has a resistivity of 10-25 Ω-m which extends to some distance horizontally.

Its thickness is about 20m. This layer may be composed of recently deposits clay. On the eastern corner of this layer is a portion which has a resistivity of 500-900Ω-m is seen with an average thickness of about 40m. Its higher resistivity shows that, it may be a lava flow from some fissural eruptions.

Next to the first layer there is a second geo-electric layer of resistivity from 20 to 30Ω.m. It has a maximum thickness of about 80m on the eastern side and a minimum thickness of about 40m near to the western side of the geo-electric section. This layer may not be different from the first layer lithologically. The difference in resistivity can be due to a difference in water concentration or compactness, the second layer being more compact.

The third geo-electric layer for this profile is the thickest layer. It has a resistivity of 50-80 Ω.m. Its exact thickness on the Western part is not known but it thins out toward the east. The maximum thickness on this side is about 80m. It may be composed of sand and gravel and is expected to be a likely aquifer bed. Next to this geo-electric layer is the fourth layer whose resistivity is in excess of 125 Ω.m. This layer might be a weathered Olivine and Alkaline basalt.

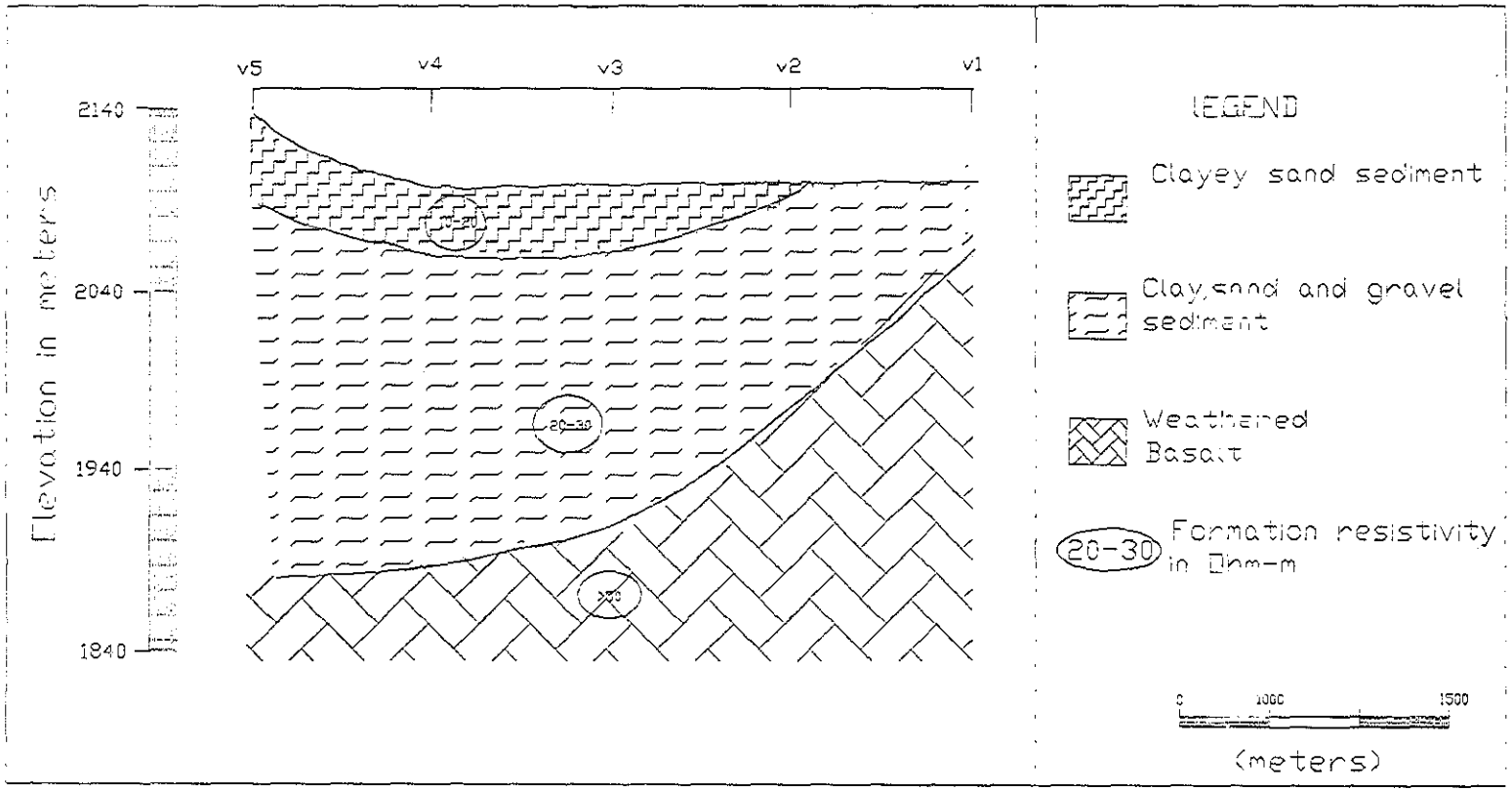

Fig.6 geo-electric section for profile 1

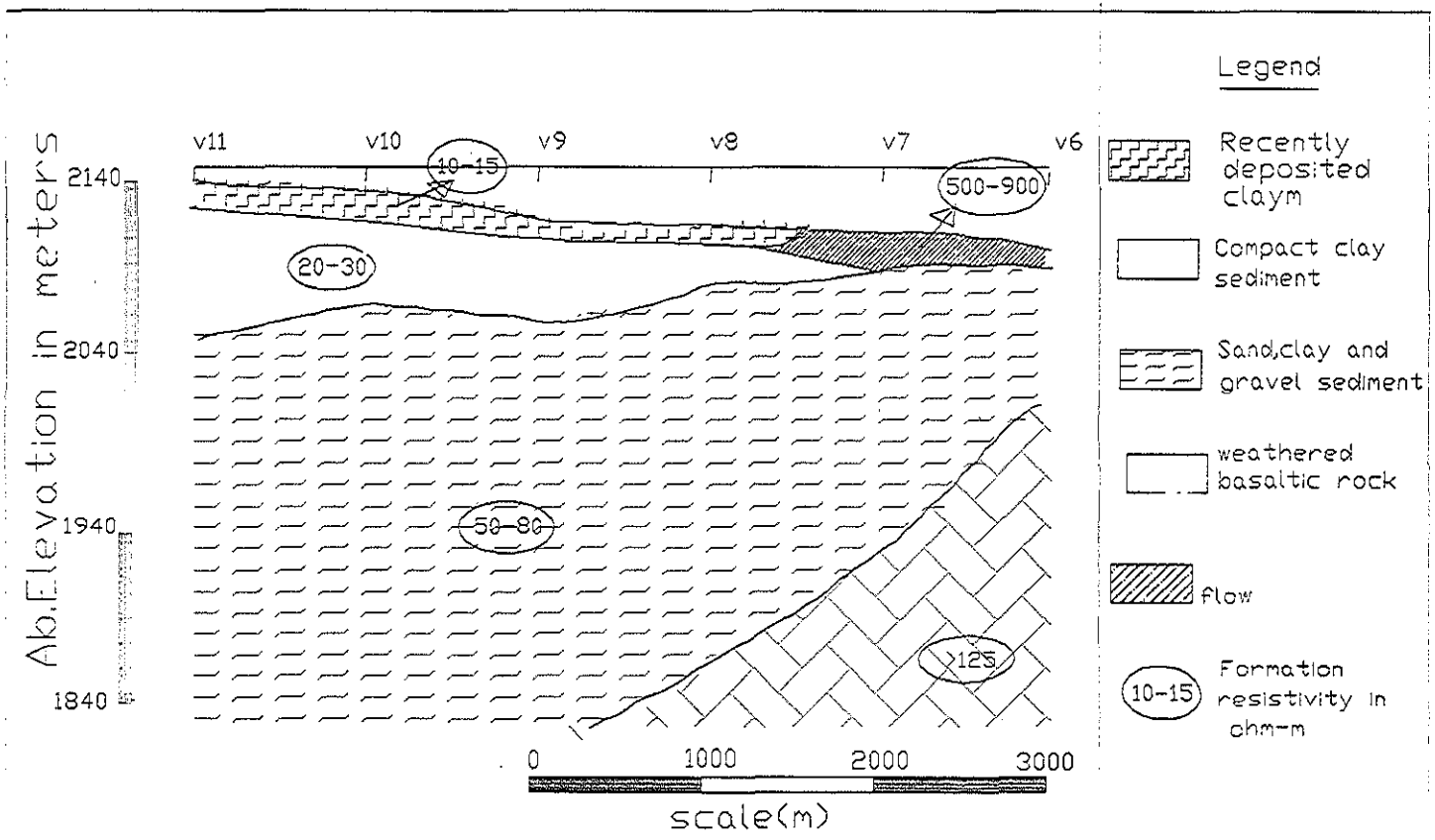

Fig.7. Geo-electric section for profile 2,Butajira.

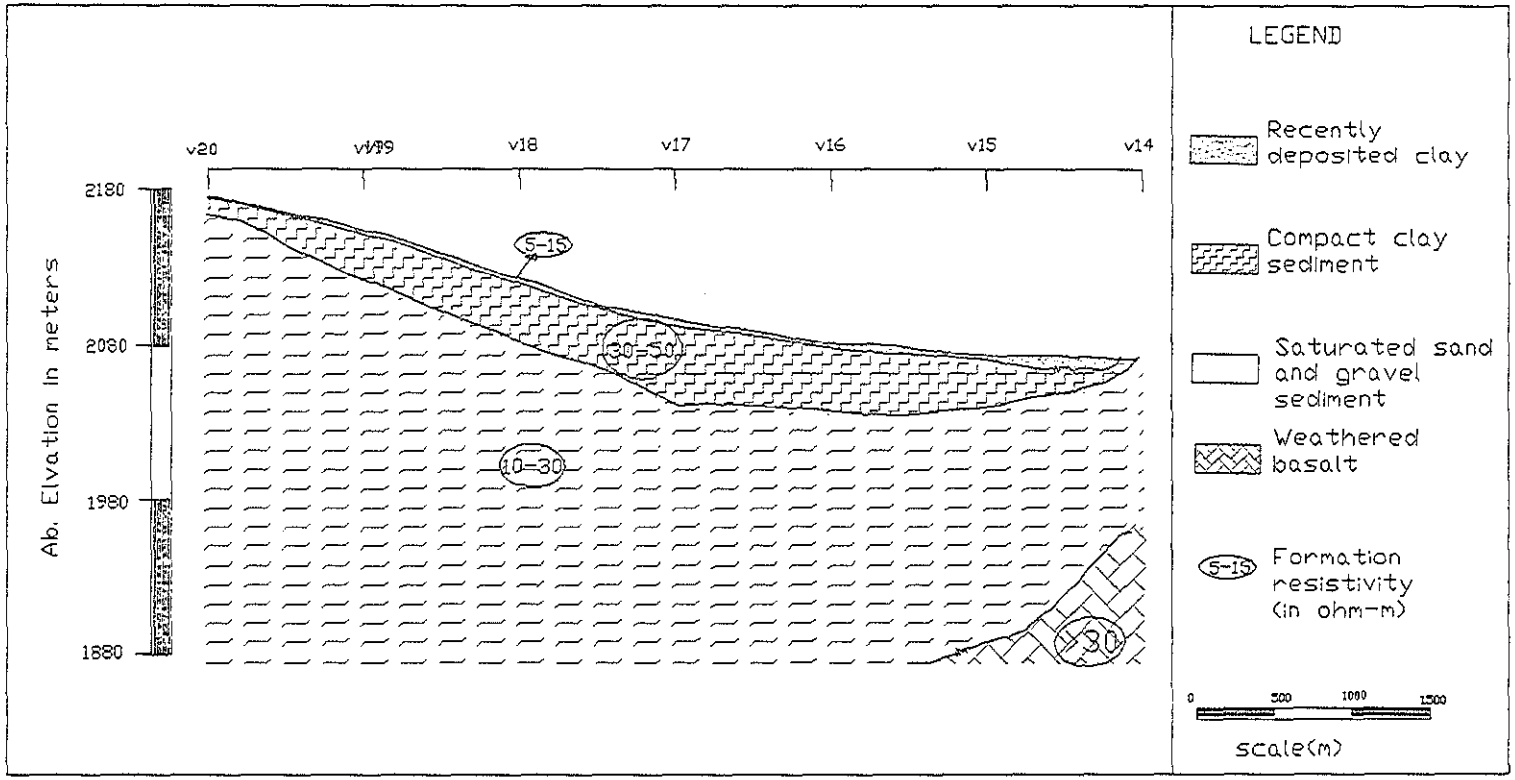

Fig.8 Geo-electric section for profile 3,Butajira

5.2.Summary and Conclusion

The practical application of the electrical resistivity method for ground water exploration has been seen. As a whole , the area seems to be rich in ground water potential. In particular, its central part of relatively low altitude has its ground water at a very shallow depth. The electrical resistivity method has shown a result consistent with . Some results are in good agreement with the information found from hand dug wells about the depth of the water table. So, the effectiveness of this method has been shown for ground water exploration in areas of similar geological set up with the Butajira area.

This work would have been more effective if there were available bore-hole data. Also, it can be recommended that the use of both electrical resistivity sounding and profiling methods together gives a better result since it makes it possible to get a good estimate of the lateral extent of the aquifer.

REFERENCES

1. Cornille, P. (1972). *Computation of Hankel transforms,* SIAM Review, 14, P.278-285.

2. Davis, P.A., Greenhalgh, S.A., Merrick, N.P. (1980). *Resistivity sounding computations with any array using a single digital filter.* Bull. Aust. Soc. Explor. Geophys, 11, P.54-62

3. Driscoll, F.G. (1989). *Ground Water and Wells.* Johnson Filtration systems Inc. Minnesota, 1089 PP,

4. Emilia, D. A, et al, (1976). *Geophysical Exploration for Ground Water in Ethiopia.* Bulletin of Geophysical Observatory, 16.

5. Gebrechristos Kassa (1985). *Physico-Mathematical Details of Electrical methods of Geophysical Prospecting and some Applications on the Analysis and Interpretation of Data from Selected Sites in Ethiopia. M.Sc. thesis , Addis Ababa University, Ethiopia.*

6. Glenn, W.E. et al, (1973). *A study of electro magnetic and resistivity sounding with an application of generalized linear inversion.* PH.D. thesis, Unversity of Utah.

7. Glenn, W.E. et al, (1973). *The inversion of vertical magentic dipole sounding data.* Geopysics, 38, P.1109-1129.

8. Hailesilassie Girmay (1985). *Shallow Resistivity Investigation In the Filwoha Fault,* M.Sc. thesis, Addis Ababa University, Ethiopia.

9. Hamilton, W.C. (1964). *Stastistics in physical science estimation, hypothesis testing, and least squares.* Ronald Press Company, New York.

10. Hoerl, A.E. and Kennard, R.W. (1970). *Ridge regression. Biased estimation for nonorthogonal problems.* Technometrics, 12, P.55-67.

11. Hoerl, A.E. (1970b). Ridge regression: *Applications to nonorthogonal problems.* Technometrics, V, 12, P. 69-82.

12. Inman, J.R. (1975). *Resistivity Inversion with Ridge Regression.* Geophysics, 40, P. 798-817.

13. Inman, J.R. Ryu, J. and Ward, S.H. (1973). *Resistivity inversion.* Geophysics, V.38 P.1088-1108.

14. Interpex Limited Golden, Co. (1992). *Resix Plus TM, v 2.2, User Manual, Resistivity Data Interpretation Soft Ware.* Interpex Limited.

15. Jenkins, G.M. and Watts, D.G. (1968). *Spectral analysis and its applications.* San Holden-Day Inc, Francisco.

16. Koefoed, O. (1979). *Geosounding Priciples, 1: Resistivity Sounding Measurements.* Elsevier, Amsterdam,

17. Kunetz, G. (1986). *Principles of direct current resistivity prospecting.* Berlin-Nikolassee, Gebruder Borntraeger.

18. Lines, L. R. and Trietel *S.A.* (1984). *Review of Least-squares Inversion and Its Application to Geophysical Problems.* Geophysical Prospecting, 32, P. 159-186.

19. Marquardt, D.W. (1963). *An algorithm for least squares estimation of nonlinear parameters.* J. Soc. Indust. Appl. Math, V11, P.431-441.

20. Marquardt, (1970). *Generalized inverses, ridge regression, biased linear estimation, and nonlinear estimation.* Technometrics, 12 P.591-612.

21. Mohr, P.A. (1971). *The Geology of Ethiopia.* Addis Ababa University Press, 268 P.

22. O'Nell, D.J. and Merrick, N.P. (1984). *A digital linear filter for resitivity sounding with a Generalized Electrode Array.* Geopysical Prospecting, 32, P.105-123.

23. Parasnis, D. S. (1978). *Principles of Applied Geophysics.* Richard Clay (The Chancer Press) Ltd, Bugay, Suffolk, 275 P.

24. Petrick, W.R. , Pelton, W.H. and Ward, S.H. (1977). *Ridge Regression Inversion Applied to Crustal Resistivity Sounding Data from South Africa.* Geophysics, 42, P. 995-1005.

25. Pilat, V.V, Jihad Abakoyas, and Abebe Ayele (1979). *Geopyhsical Investigation for Ground Water in Butajira town.* Ethiopian Institute of Geological Studies, Addis Ababa, Ethiopia.

26. Ralston, A. (1965). *A first course in numerical analysis.* McGraw-Hill Book Co., New York,

27. Rijo, L. et al (1977). *Interpretation of Apparent Resistivity Data from Apodi Valley, Grande De Norte, Brazil.* Geophysics 42, P. 811-822.

28. Sebsibe Alemneh (1994). *South West Butajira Drinking Water Project Proposal.* Addis Ababa, Ethiopia.

29. Schellinger, D.K. (1972). *Curie depth determinations in the High Plateaus, Utah.* M.Sc. thesis, University of Utah.

30. Shuey, R.T. (1973). *Comments on the paper, "Interpretation of gravity anomalies by nonlinear optimization" by Mahboub Al-Chalabi.* Geophysics. Prosp (submitted for publication).

31. Sunde, E.D. (1949). *Earth conduction effects in transmission systems.* Van Nos-trand, New York, P.55.

32. Telford, W. M. et al (1976). *Applied Geophysics. Cambridge University Press, Cambridge,*

33. Tesfaye Chernet (1985). *Hydrogeology of the Lakes Region.* Ethiopian Mapping Agency, Addis Ababa.

34. Wiggins, R.A. (1972). *The general linear inverse problem. Implication of surface waves and free oscillations for earth structure.* Rev. Geophys. and space Phys. 10, P.251-285.

35. Zohdy, A.A.R (1989). *A New Method for the Automatic Interpretation of Schlumberger and Wenner Sounding Curves.* Geophysics, 54, P. 245-253.

APPENDIX

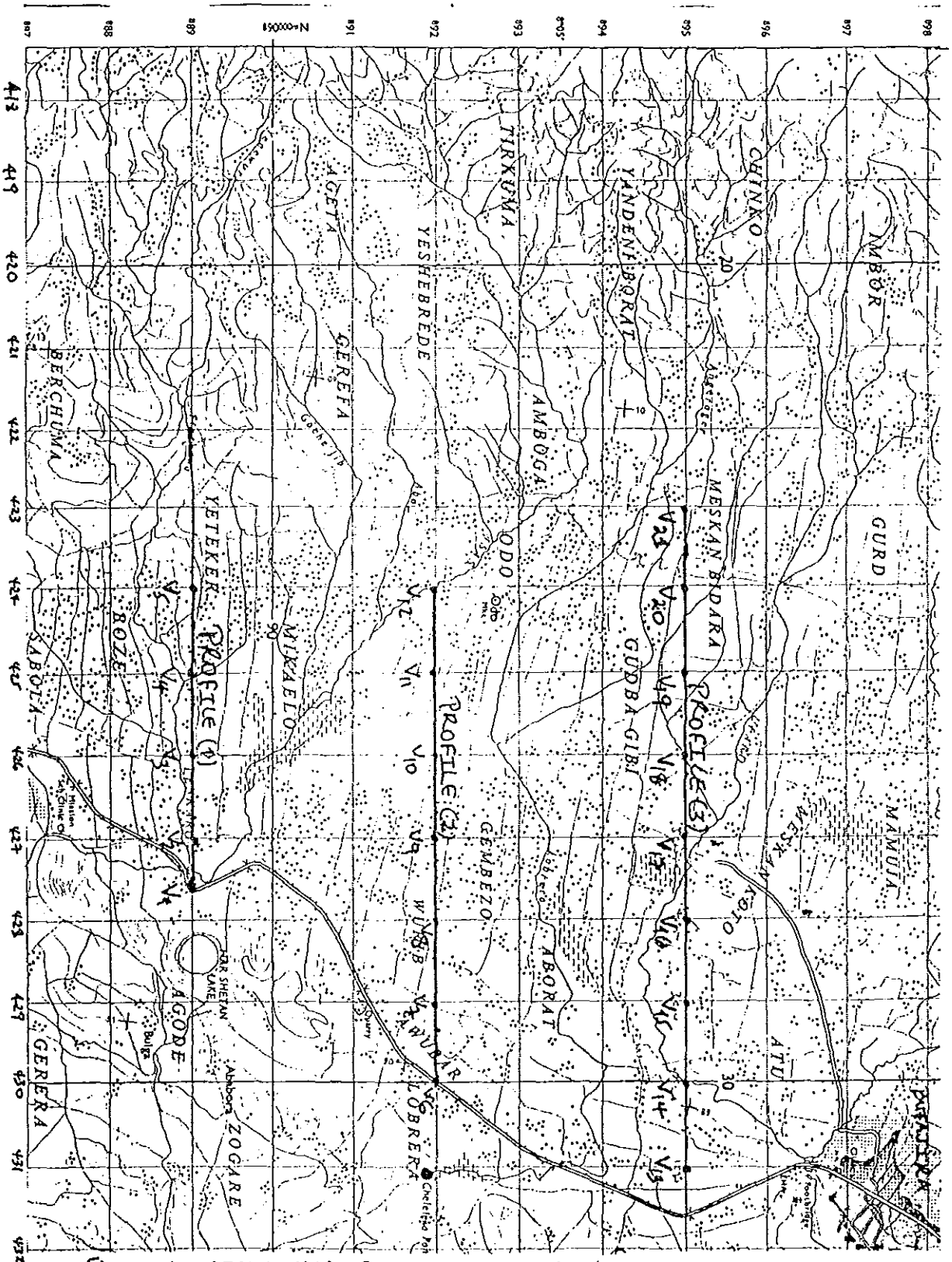

Fig. A.1. LOCATION MAP OF THE SURVEY AREA

DATA SET: V_1, Profile 1
CONFIGURATION: SCHLUMBERGER
DATE: FEBRUARY, 1997

No.	AB/2 (m)	RHO-A (ohm-m)
1	1.5	25.30
2	2.1	29.40
3	3.0	26.50
4	4.2	24.70
5	6.0	24.30
6	9.0	32.20
7	13.5	39.40
8	20.0	50.70
9	45.0	67.50
10	66.0	68.90
11	100.0	55.70

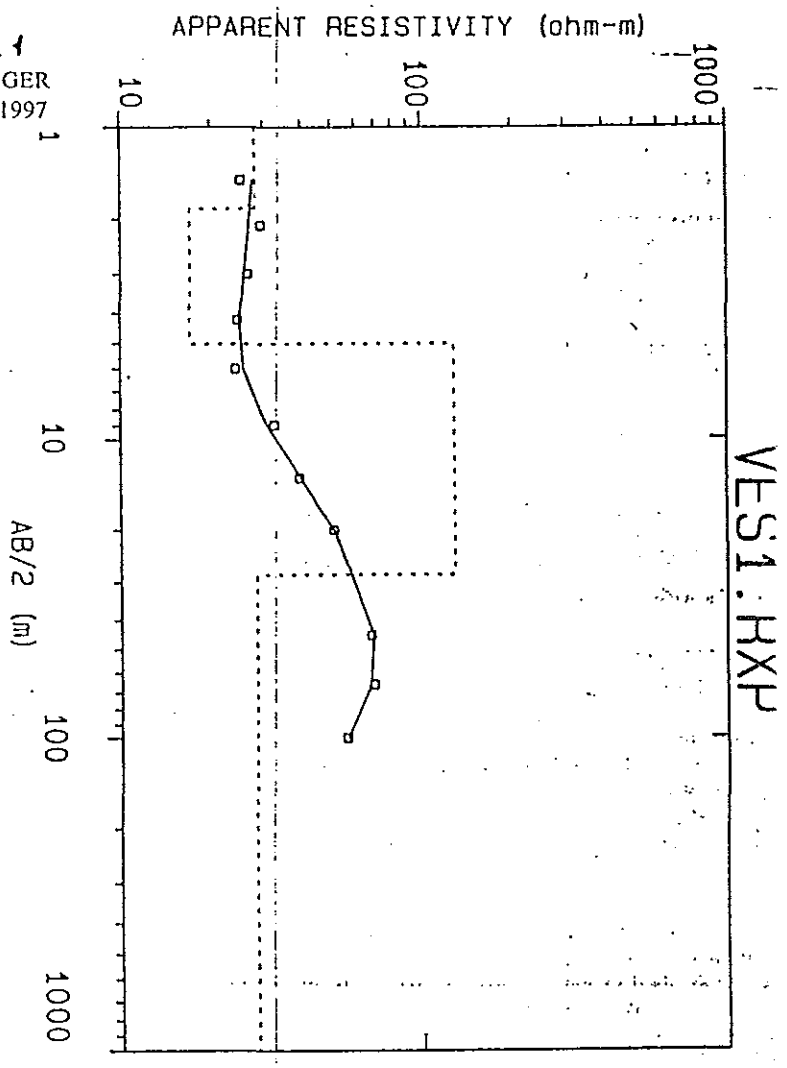

INTERPRETATION
FITTING ERROR: 4.705 PERCENT

Layer No.	Resistivity (Ohm-m)	Thickness (m)	Depth (m)
1	28.14	1.85	1.85
2	6.85	3.15	5.00
3	128.6	23.32	28.32
4	28.16	Infinitive	Infinitive

Fig. A-2. Interpretation Result of V_1

DATA SET: V_2, Profile 1
CONFIGURATION: SCHLUMBERGER
DATE: FEBRUARY, 1997

No.	AB/2 (m)	RHO-A (ohm-m)
1	1.5	16.00
2	2.1	15.96
3	3.0	18.79
4	4.2	19.00
5	6.0	19.11
6	9.0	16.24
7	13.5	16.59
8	20.0	16.03
9	30.0	18.06
10	45.0	19.00
11	66.0	18.00
12	100.0	19.00
13	150.0	20.50
14	220.0	24.00

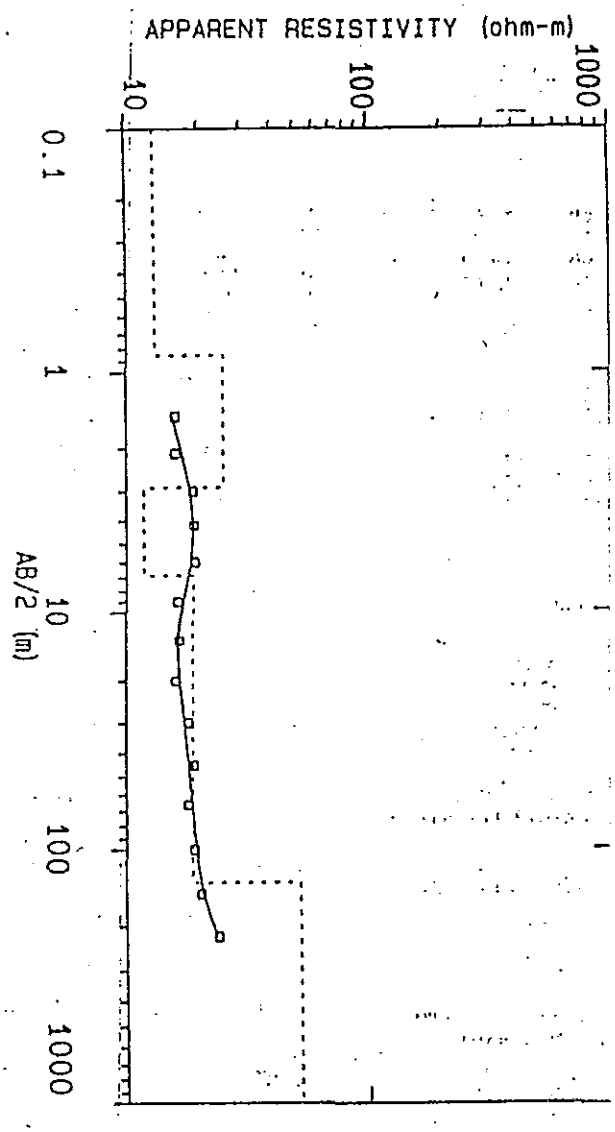

INTERPRETATION
FITTING ERROR: 3.549 PERCENT

Layer No.	Resistivity (Ohm-m)	Thickness (m)	Depth (m)
1	13.13	0.849	0.849
2	25.23	2.04	2.89
3	11.82	3.95	6.84
4	18.84	128.50	135.30
5	52.68	Infinitive	Infinitive

Fig. A-3. Interpretation Result of V_2.

DATA SET: V4, Profile 1
CONFIGURATION: SCHLUMBERGER
DATE: FEBRUARY, 1997

No.	AB/2 (m)	RHO-A (ohm-m)
1	1.5	17.40
2	2.1	16.26
3	3.0	14.60
4	4.2	13.06
5	6.0	11.39
6	9.0	11.63
7	13.5	12.00
8	20.0	13.54
9	30.0	14.03
10	45.0	14.50
11	66.0	16.00
12	100.0	22.00
13	150.0	26.00
14	220.0	32.00
15	330.0	38.00
16	500.0	58.00

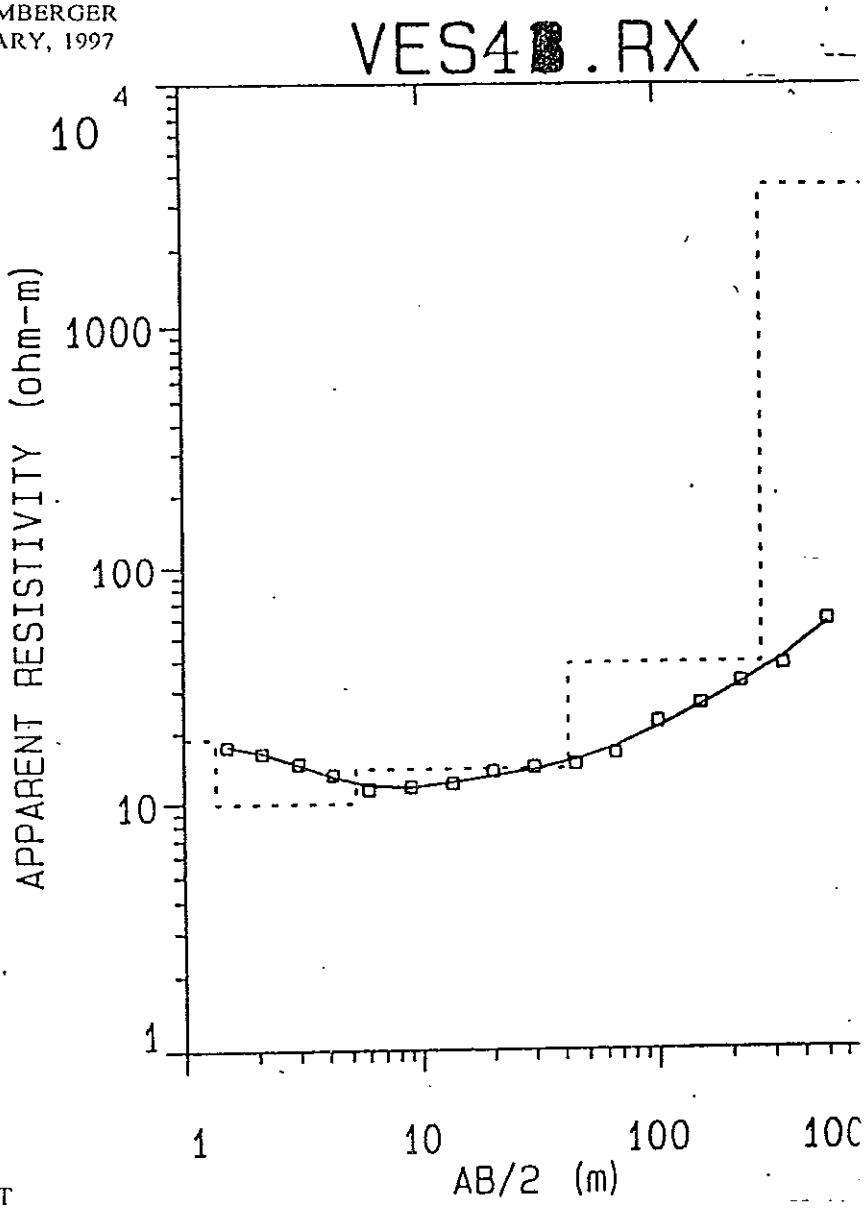

INTERPRETATION
FITTING ERROR: 3.522 PERCENT

Layer No.	Resistivity (Ohm-m)	Thickness (m)	Depth (m)
1	18.78	1.33	1.33
2	9.94	3.93	5.27
3	13.88	36.46	41.73
4	38.67	226.50	268.20
4	3621.90	Infinitive	Infinitive

Fig. A.4. Interpretation Result of V4.

DATA SET: Vs, Profile 1
CONFIGURATION: SCHLUMBERGER
DATE: FEBRUARY, 1997

No.	AB/2 (m)	RHO-A (ohm-m)
1	1.5	12.50
2	2.1	11.00
3	3.0	10.50
4	4.2	10.56
5	6.0	11.33
6	9.0	11.34
7	13.5	13.26
8	20.0	13.71
9	30.0	14.41
10	45.0	16.00
11	66.0	17.00
12	100.0	18.50
13	150.0	20.00
14	220.0	24.00
15	330.0	26.00
16	500.0	31.00

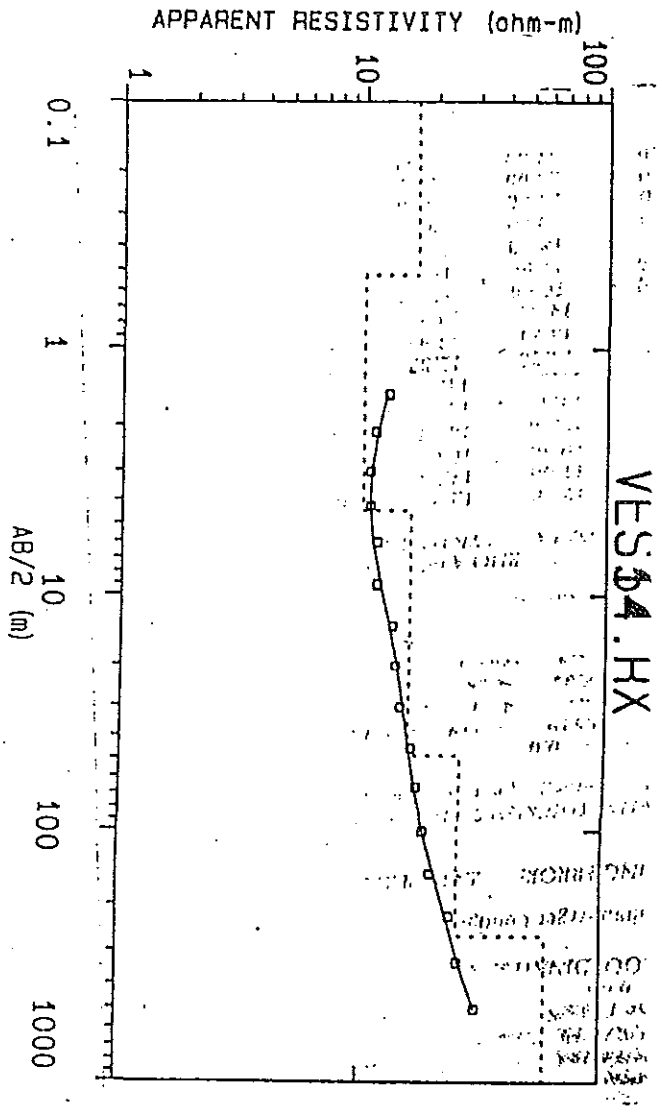

INTERPRETATION
FITTING ERROR: 2.410 PERCENT

Layer No.	Resistivity (Ohm-m)	Thickness (m)	Depth (m)
1	16.45	0.519	0.519
2	9.81	3.87	4.39
3	15.65	44.02	48.41
4	25.82	212.90	261.30
5	60.13	Infinitive	Infinitive

Fig. A.5. Interpretation Result of Vs.

DATA SET: V6, Profile 2
CONFIGURATION: SCHLUMBERGER
DATE: FEBRUARY, 1997

No.	AB/2 (m)	RHO-A (ohm-m)
1	1.5	39.00
2	2.1	46.00
3	3.0	51.00
4	4.2	67.13
5	6.0	92.20
6	9.0	128.5
7	13.5	184.0
8	20.0	222.0
9	30.0	234.0
10	45.0	200.0
11	66.0	140.0
12	100.0	70.00
13	150.0	43.00
14	220.0	39.00
15	330.0	50.00
16	500.0	65.00

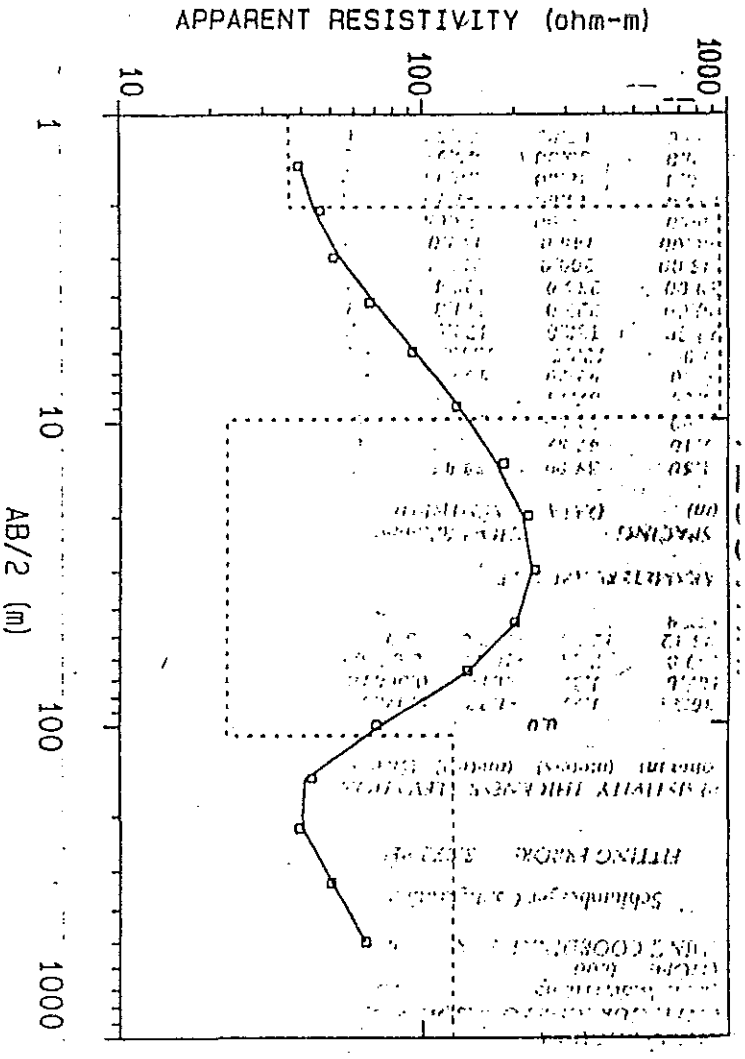

INTERPRETATION
FITTING ERROR: 3.369 PERCENT

Layer No.	Resistivity (Ohm-m)	Thickness (m)	Depth (m)
1	36.27	2.04	2.04
2	942.70	7.75	9.80
3	22.45	98.07	107.80
4	125.20	Infinitive	Infinitive

Fig. A.6. Interpretation Result of V6.

DATA SET: V_7, Profile 2
CONFIGURATION: SCHLUMBERGER
DATE: FEBRUARY, 1997

No.	AB/2 (m)	RHO-A (ohm-m)
1	1.5	60.00
2	2.1	60.00
3	3.0	64.00
4	6.0	87.00
5	9.0	108.00
6	13.50	144.80
7	20.00	180.0
8	30.0	217.0
9	45.0	220.00
10	66.00	190.0
11	100.0	100.00
12	150.0	44.00
13	220.0	20.00

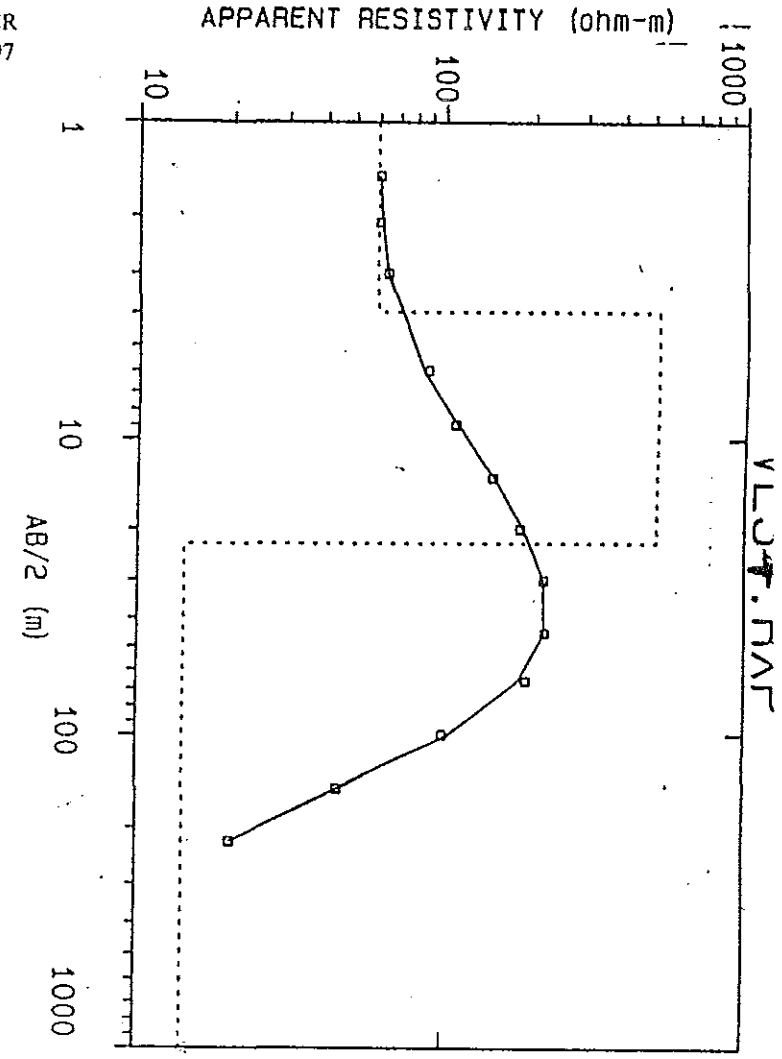

INTERPRETATION
FITTING ERROR: 2.598 PERCENT

Layer No.	Resistivity (Ohm-m)	Thickness (m)	Depth (m)
1	59.19	3.97	3.97
2	515.0	18.39	22.36
3	14.09	Infinitive	Infinitive

Fig. A.7. Interpretation result of V_7.

DATA SET: V8 , Profile 2
CONFIGURATION: SCHLUMBERGER
DATE: FEBRUARY, 1997

No.	AB/2 (m)	RHO-A (ohm-m)
1	1.5	7.24
2	2.1	7.46
3	3.0	7.50
4	4.2	8.00
5	6.0	9.66
6	9.0	10.76
7	13.5	14.00
8	45.0	19.50
9	66.0	24.00
10	100.0	29.00
11	150.0	38.00
12	220.0	41.50
13	330.0	51.50
14	500.0	65.00

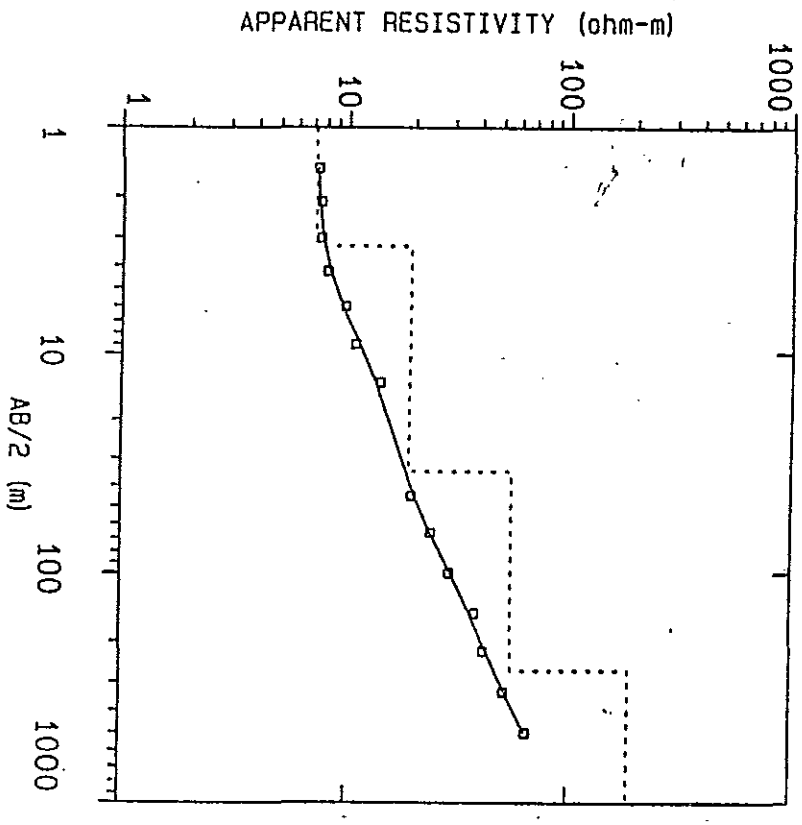

INTERPRETATION
FITTING ERROR: 3.008 PERCENT

Layer No.	Resistivity (Ohm-m)	Thickness (m)	Depth (m)
1	7.12	3.26	3.26
2	18.98	31.40	34.66
3	55.21	231.2	265.8
4	187.3	Infinitive	Infinitive

Fig. A.8. Interpretation Result of V8

DATA SET: Vq; Profile 2
CONFIGURATION: SCHLUMBERGER
DATE: FEBRUARY, 1997

No.	AB/2 (m)	RHO-A (ohm-m)
1	1.5	13.47
2	2.1	11.21
3	3.0	10.39
4	4.2	9.30
5	6.0	9.66
6	9.0	10.01
7	13.5	12.95
8	20.0	18.55
9	30.0	19.79
10	45.0	22.00
11	66.0	23.53
12	100.0	27.02
13	150.0	33.63
14	220.0	39.67
15	330.0	48.85
16	500.0	57.58

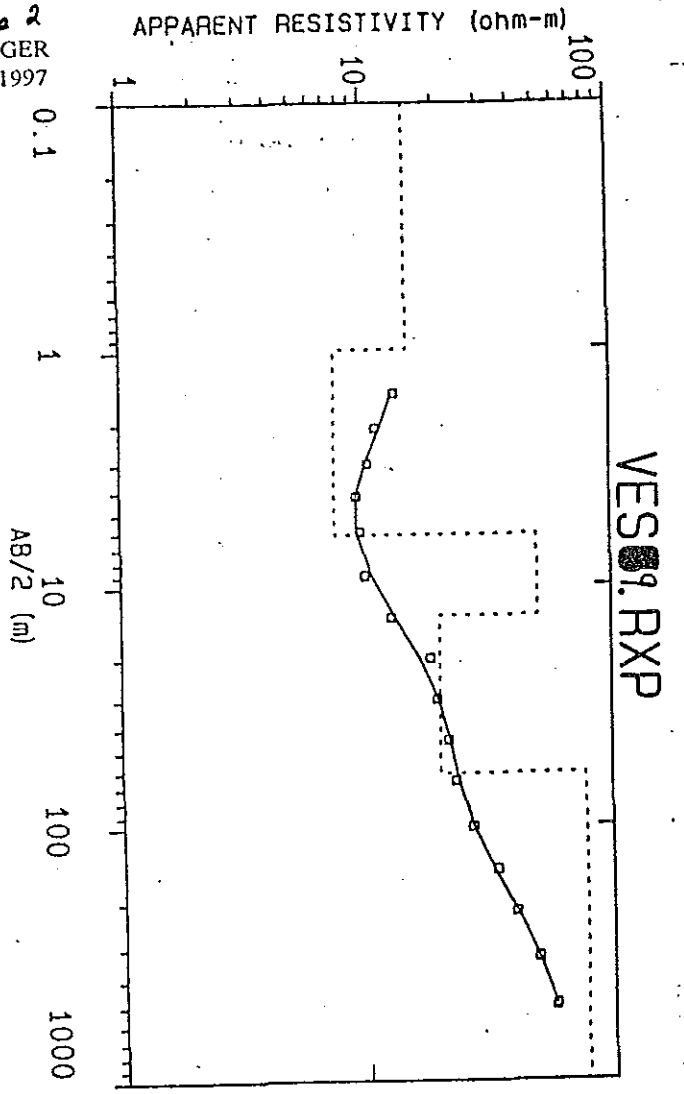

INTERPRETATION
FITTING ERROR: 3.802 PERCENT

Layer No.	Resistivity (Ohm-m)	Thickness (m)	Depth (m)
1	15.24	0.993	0.993
2	7.53	5.14	6.13
3	50.00	7.07	13.21
4	20.25	48.55	61.76
5	77.54	Infinitive	Infinitive

Fig. A.9. Interpretation Result of Vq.

DATA SET: V10, Profile 2
CONFIGURATION: SCHLUMBERGER
DATE: FEBRUARY, 1997

No.	AB/2 (m)	RHO-A (ohm-m)
1	1.5	25.49
2	2.1	31.72
3	3.0	31.72
4	4.2	25.85
5	6.0	20.56
6	9.0	14.11
7	13.5	10.50
8	20.0	9.26
9	30.0	11.05
10	45.0	15.07
11	66.0	17.53
12	100.0	20.98
13	150.0	26.69
14	220.0	32.67
15	330.0	42.16
16	500.0	45.40

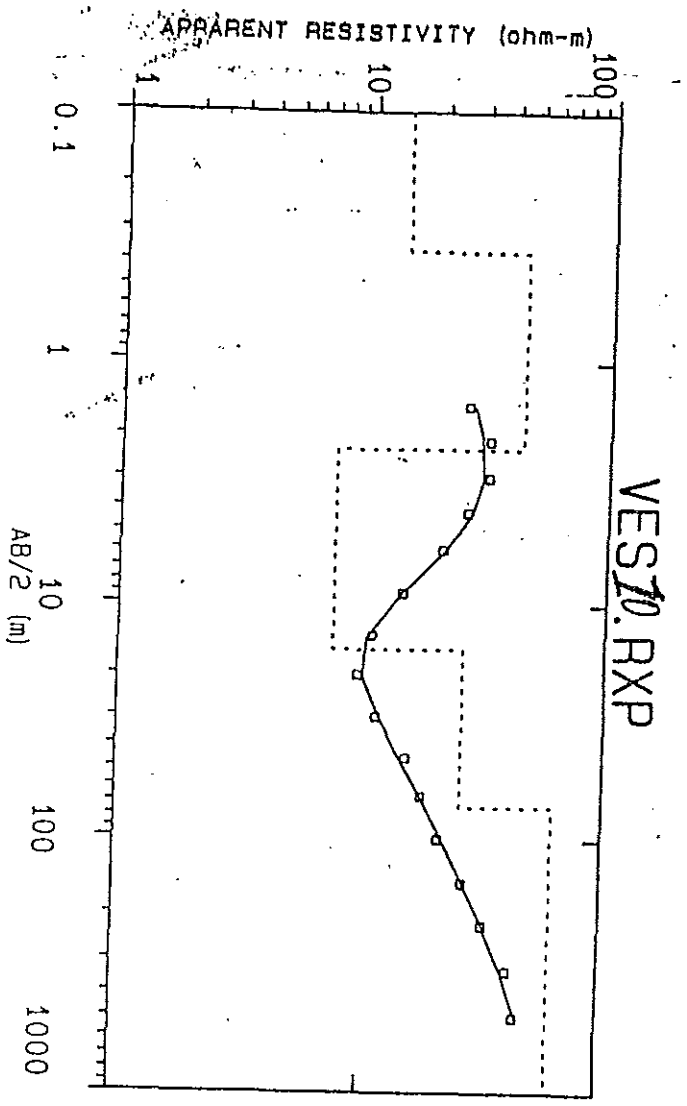

INTERPRETATION
FITTING ERROR: 4.359 PERCENT

Layer No.	Resistivity (Ohm-m)	Thickness (m)	Depth (m)
1	13.90	0.362	0.362
2	43.84	1.900	2.260
3	7.28	13.180	15.450
4	25.59	57.480	72.930
5	62.40	Infinitive	Infinitive

Fig. A-10. Interpretation Result of V_{10}.

DATA SET: V_{II}, Profile 2
CONFIGURATION: SCHLUMBERGER
DATE: FEBRUARY, 1997

No.	AB/2 (m)	RHO-A (ohm-m)
1	1.5	10.14
2	2.1	10.37
3	3.0	10.68
4	4.20	10.77
5	6.0	10.90
6	9.00	11.31
7	13.50	11.56
8	20.0	14.00
9	30.0	18.00
10	45.00	25.00
11	66.00	30.00
12	100.0	32.00
13	150.0	34.00
14	220.0	40.00
15	330.0	46.00
16	500.0	50.00

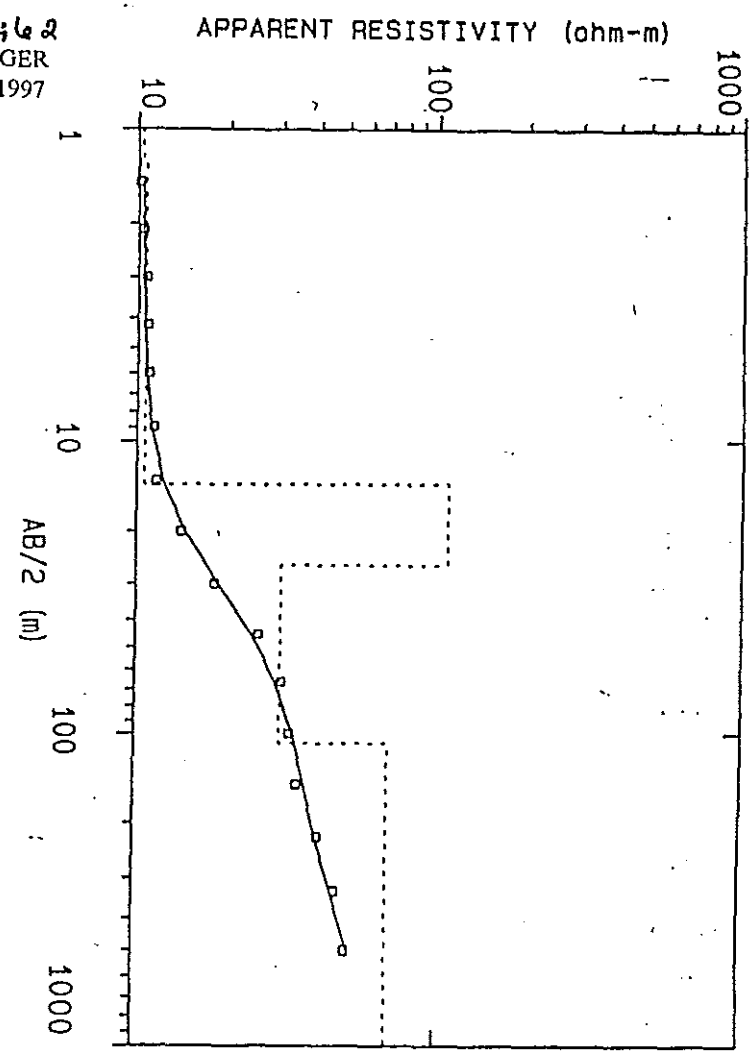

INTERPRETATION
FITTING ERROR: 3.294 PERCENT

Layer No.	Resistivity (Ohm-m)	Thickness (m)	Depth (m)
1	10.33	1.32	1.32
2	10.60	12.48	13.81
3	107.9	12.15	25.97
4	29.71	82.04	108.0
5	68.34	Infinitive	Infinitive

Fig. A-11. Interpretation Result of V_{II}

DATA SET: V15, Profile 3
CONFIGURATION: SCHLUMBERGER
DATE: FEBRUARY, 1997

No.	AB/2 (m)	RHO-A (ohm-m)
1	1.5	5.45
2	2.1	5.40
3	3.0	5.78
4	4.2	6.15
5	6.0	7.03
6	9.0	7.68
7	13.5	9.91
8	45.0	16.43
9	66.0	20.13
10	100.0	25.00
11	150.0	29.95
12	220.0	34.30
13	330.0	49.00

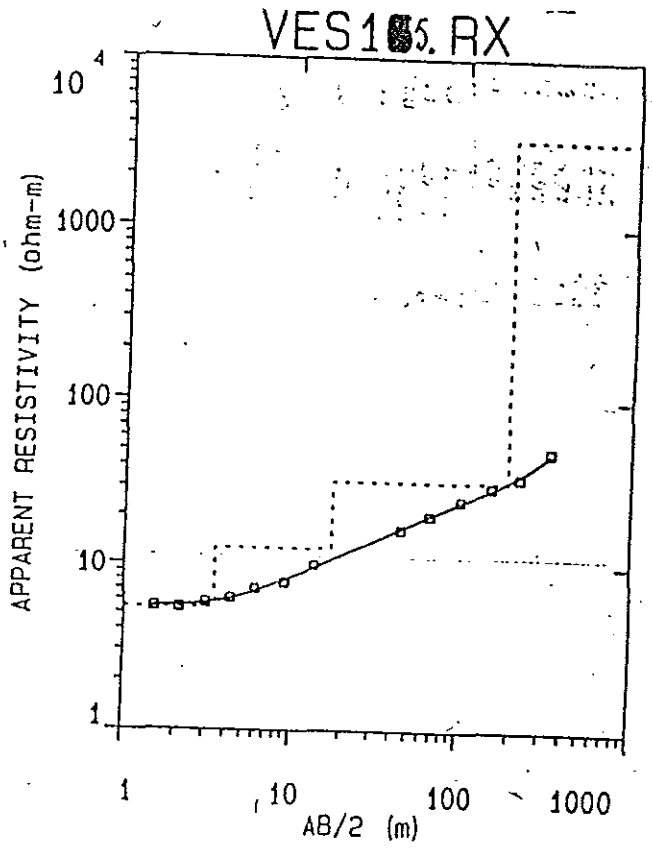

INTERPRETATION
FITTING ERROR: 2.684 PERCENT

Layer No.	Resistivity (Ohm-m)	Thickness (m)	Depth (m)
1	5.41	3.39	3.39
2	12.53	13.68	17.08
3	32.15	171.60	188.70
4	3259.10	Infinitive	Infinitive

Fig. A. 13. Interpretation Result of V15.

DATA SET: V_{17} Profile 3
CONFIGURATION: SCHLUMBERGER
DATE: FEBRUARY, 1997

No.	AB/2 (m)	RHO-A (ohm-m)
1	1.5	11.52
2	2.1	10.85
3	3.0	10.30
4	4.2	9.80
5	6.0	9.50
6	9.0	10.00
7	13.5	12.00
8	20.0	14.40
9	30.0	17.30
10	45.0	18.30
11	66.0	20.30
12	100.0	25.00
13	150.0	27.00
14	220.0	32.00
15	330.0	34.00

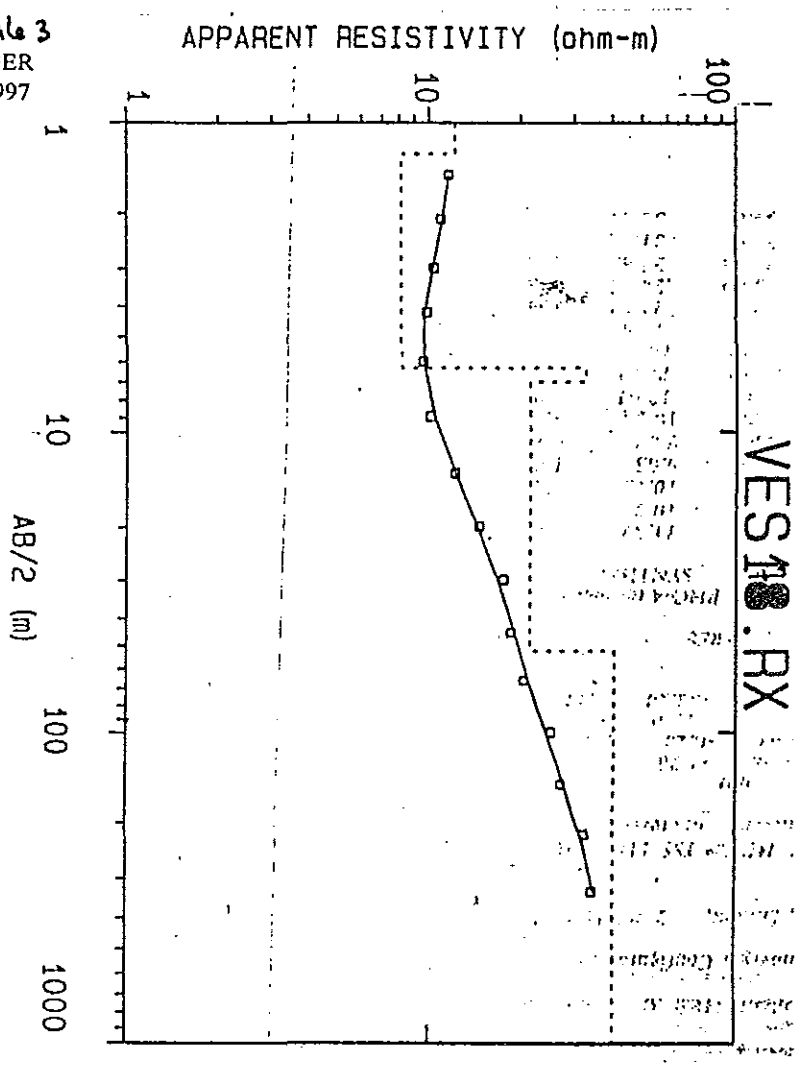

INTERPRETATION
FITTING ERROR: 2.380 PERCENT

Layer No.	Resistivity (Ohm-m)	Thickness (m)	Depth (m)
1	12.11	1.26	1.26
2	8.09	5.01	6.28
3	32.18	0.727	7.00
4	21.36	45.23	52.24
4	40.14	Infinitive	Infinitive

Fig. A·14. Interpretation Result of V_{17}.

DATA SET: V19 Profil 3
CONFIGURATION: SCHLUMBERGER
DATE: FEBRUARY, 1997

No.	AB/2 (m)	RHO-A (ohm-m)
1	1.5	12.03
2	2.1	10.40
3	3.0	9.00
4	4.2	7.70
5	6.0	7.20
6	9.0	7.08
7	13.5	7.06
8	20.0	7.00
9	30.0	6.70
10	66.0	6.80
11	100.0	7.00
12	150.0	7.00
13	220.0	7.50
14	330.0	8.00
15	500.0	9.00

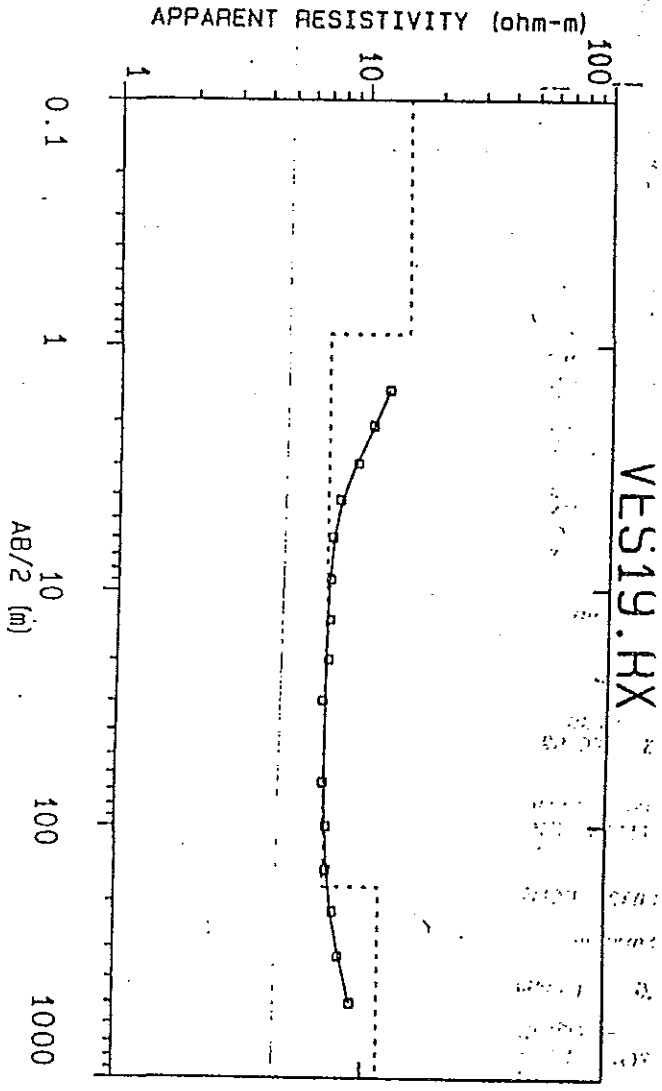

INTERPRETATION
FITTING ERROR: 1.330 PERCENT

Layer No.	Resistivity (Ohm-m)	Thickness (m)	Depth (m)
1	14.59	0.897	0.897
2	6.85	175.100	176.000
3	11.66	Infinitive	Infinitive

Fig. A. 15. Interpretation Result of V19

DATA SET: V_{20}, Profile 3
CONFIGURATION: SCHLUMBERGER
DATE: FEBRUARY, 1997

No.	AB/2 (m)	RHO-A (ohm-m)
1	1.5	21.30
2	2.1	20.66
3	3.0	22.00
4	4.2	24.00
5	6.0	27.02
6	9.0	31.00
7	13.5	33.50
8	20.0	30.00
9	30.0	25.00
10	45.0	18.00
11	66.0	15.00
12	100.0	13.65
13	150.0	12.50
14	220.0	13.00
15	330.0	14.00
16	500.0	15.00

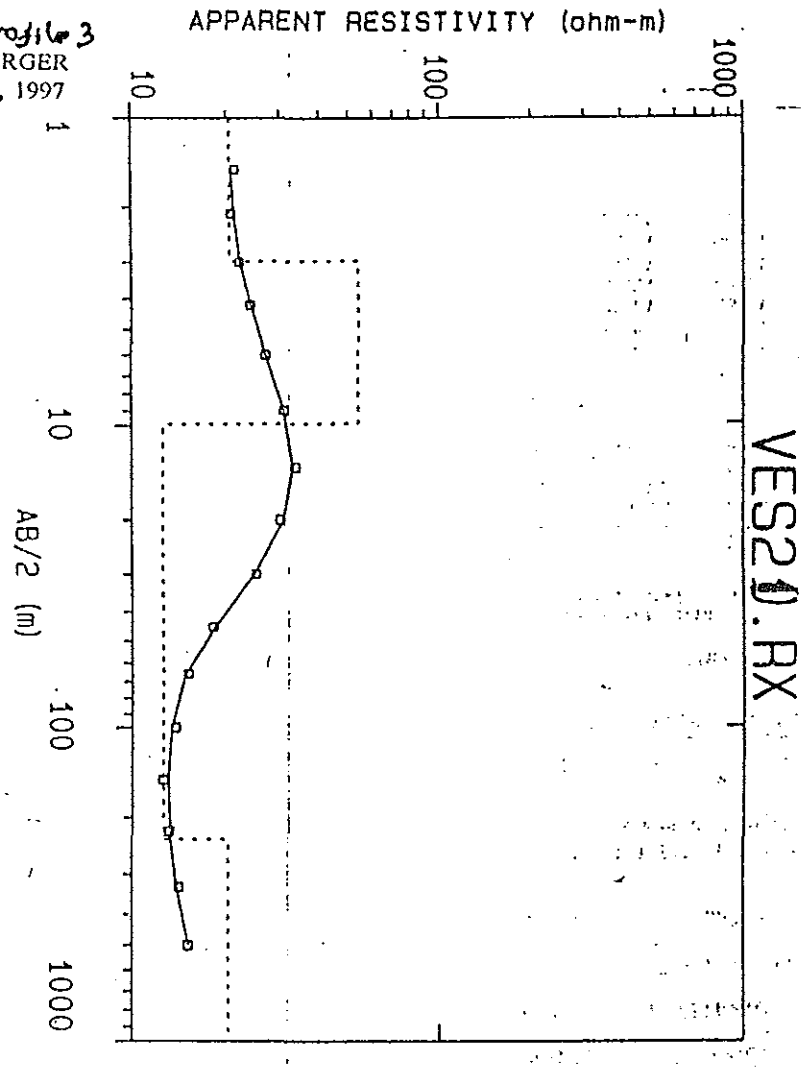

INTERPRETATION
FITTING ERROR: 1.867 PERCENT

Layer No.	Resistivity (Ohm-m)	Thickness (m)	Depth (m)
1	20.47	2.98	2.98
2	53.89	6.94	9.92
3	12.49	223.10	233.00
4	20.18	Infinitive	Infinitive

Fig. A-16. Interpretation Result of V_{20}

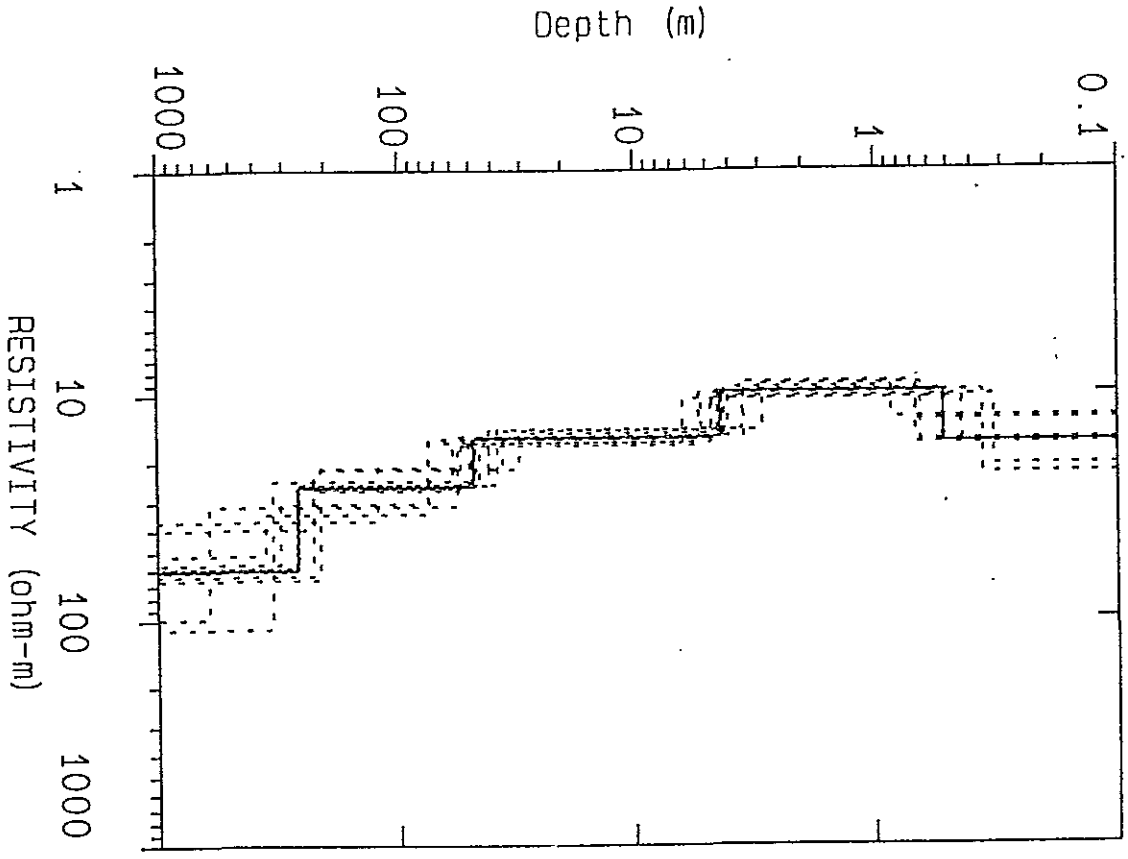

Fig. A.17. Equivalent Analysis Result of V_S.

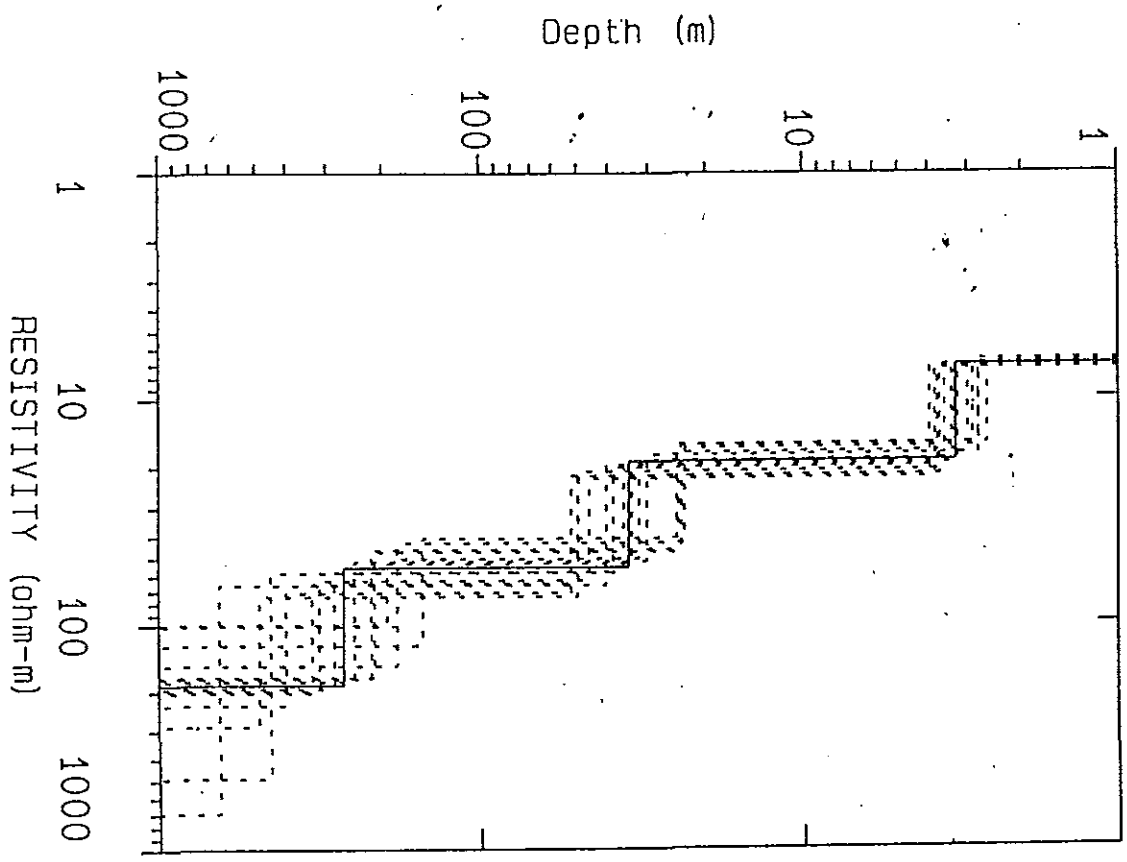

Fig. A.18. Equivalent Analysis Result of V_8.

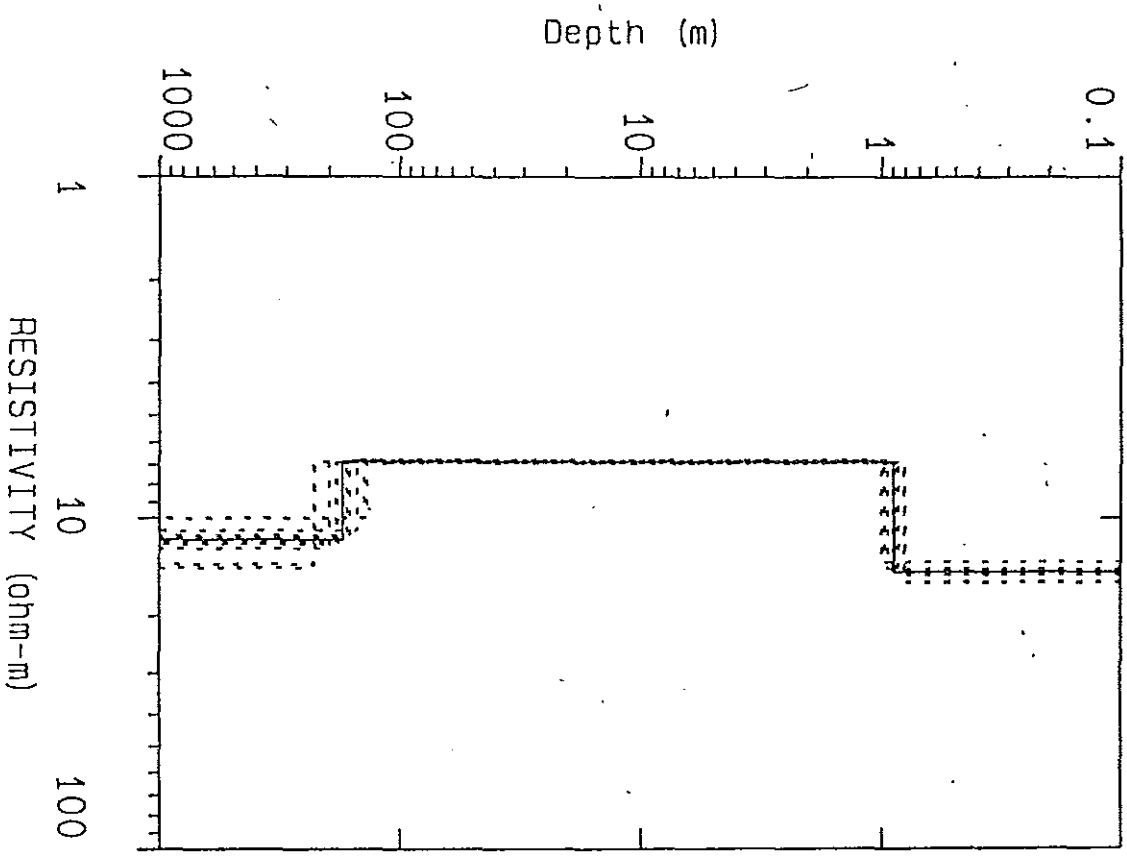

Fig. A.19. Equivalent Analysis Result of V_{19}.

* *Rural Community Water Dept., Ethi*

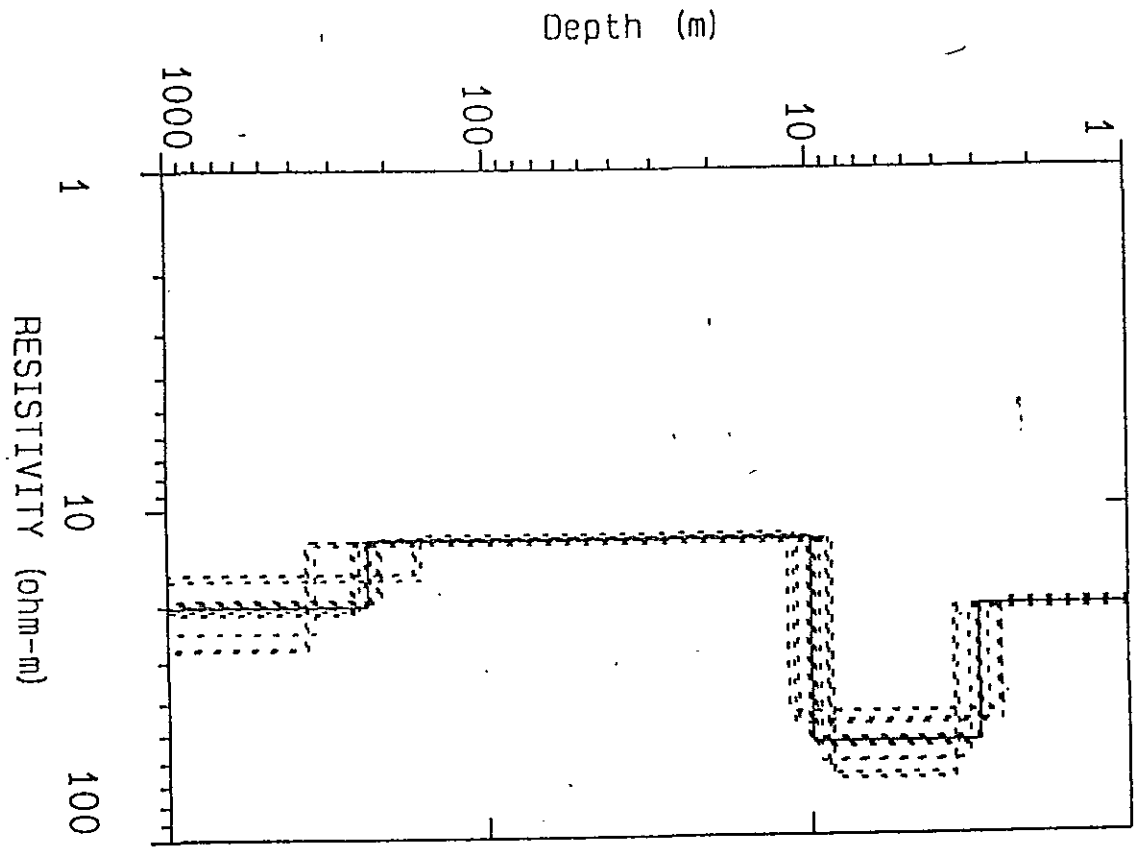

Fig. A.20. Equivalent Analysis Result of V_{20}

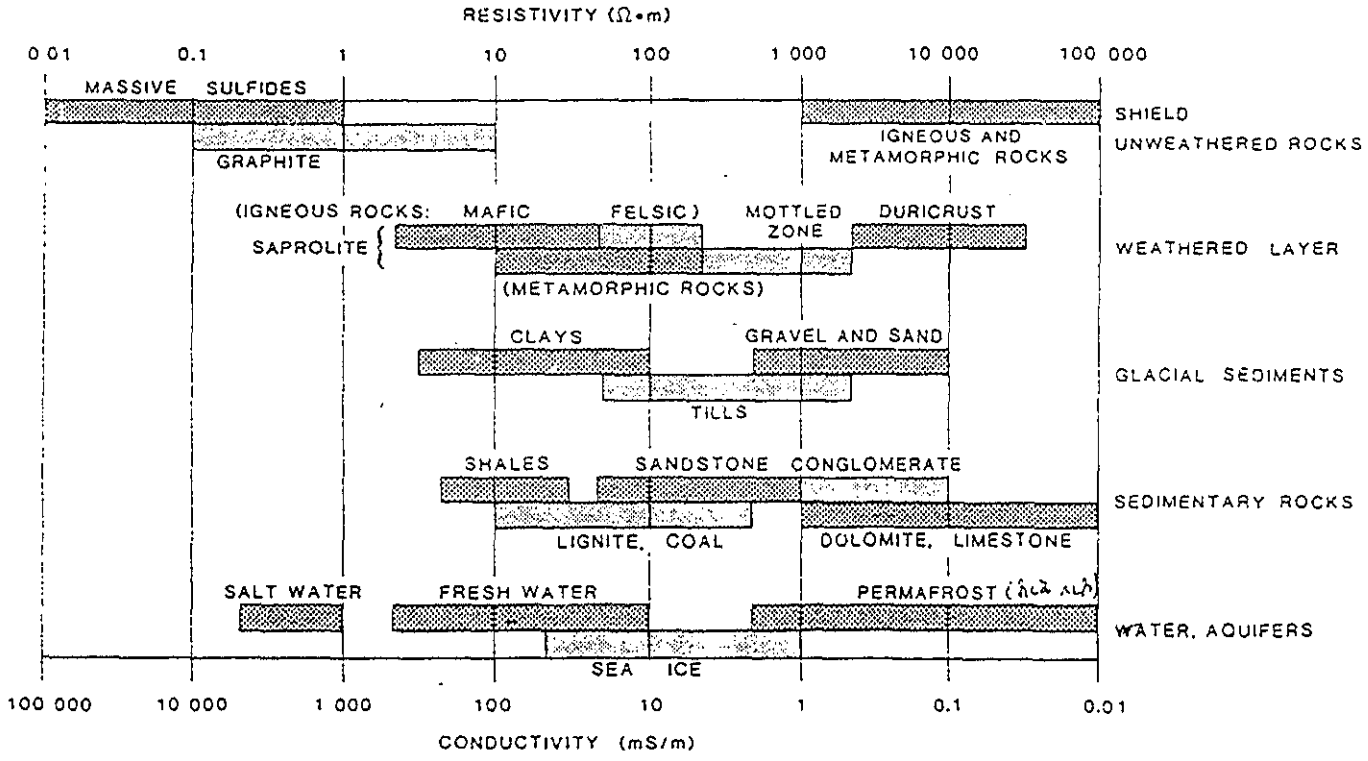

Fig A.25. Typical ranges of resistivities of earth materials.